Pb isotopes and geochemical monitoring of Arctic sedimentary supplies and water mass export through Fram Strait since the Last Glacial Maximum

Jenny Maccali, Claude Hillaire-Marcel, Jean Carignan, Laurie Reisberg

Pb isotopes and geochemical monitoring of Arctic sedimentary supplies and water mass export through Fram Strait since the Last Glacial Maximum

Jenny Maccali,[1,2] Claude Hillaire-Marcel,[1] Jean Carignan,[3] and Laurie C. Reisberg[4]

Received 4 April 2011; revised 13 October 2011; accepted 17 October 2011; published 6 January 2012.

[1] Elemental and Pb isotope measurements were performed on leachates and residues from surface sediments and two <50 cm cores (MC04 and MC16) collected along a NE-SW transect through Fram Strait. Geochemical and isotopic properties of residues from surface sediments define three distinct spatial domains within the Strait: 1) the easternmost edge of the Strait; 2) the eastern part of the Strait off the Svalbard margins; and 3) the western part of the Strait, influenced by supplies from Svalbard, the Nordic seas with possible contributions from northwestern Siberian margins, and sea ice and water outflow from the Arctic, respectively. Core MC16, in the third domain beneath the outflowing Arctic waters, spans the Last Glacial Maximum present interval. Sediments from this core were leached to obtain detrital (residues) and exchangeable (leachates) fractions. Detrital supplies to core MC16 are believed to originate mainly from melting of the overlying sea ice and thus can be used to document changes in Arctic sedimentary sources. Detrital $^{206}Pb/^{204}Pb$ and $^{208}Pb/^{206}Pb$ ratios illustrate two mixing trends, Trends A and B, corresponding to the pre- and post-Younger Dryas (YD) intervals, respectively. These trends represent binary mixtures with a common end-member (Canadian margins) and either a Siberian (Trend A) or Greenland (Trend B) margin end-member. The YD is marked by an isotopic excursion toward the Canadian end-member, suggesting a very active Beaufort Gyre possibly triggered by massive drainage of the Laurentide ice sheet. Pb isotope compositions of leachates, thought to represent the signature of the overlying water masses, define a unique linear trend coincident with Trend A. This suggests that water masses acquired their signature through exchange with particulate fluxes along the Canadian and Siberian continental margins.

Citation: Maccali, J., C. Hillaire-Marcel, J. Carignan, and L. C. Reisberg (2012), Pb isotopes and geochemical monitoring of Arctic sedimentary supplies and water mass export through Fram Strait since the Last Glacial Maximum, *Paleoceanography*, *27*, PA1201, doi:10.1029/2011PA002152.

1. Introduction

[2] Freshwater/sea ice exports from the Arctic into the North Atlantic have a direct impact on the Atlantic Meridional Overturning Circulation (AMOC) and thus on the circum-Atlantic climate [*Broecker*, 1991; *Broecker and Peng*, 1992; *McManus et al.*, 2004; *Peltier et al.*, 2006]. Fram Strait, situated between Greenland and Spitsbergen, the main and westernmost island of the Svalbard Archipelago, is the only deep gateway allowing passage of North Atlantic Water (NAW) as a subsurface water mass into the Arctic [*Rudels et al.*, 2004]. It is also the major route of freshwater/sea ice export into the North Atlantic and its marginal basins [*Fahrbach et al.*, 2001; *Hebbeln and Wefer*, 1997; *Jones et al.*, 1995; *Rudels et al.*, 2005]. Documentation of water mass exchange through this strait, using geochemical and sedimentological records in deep-sea cores, may thus help elucidate the influence of Arctic sea ice or freshwater export on the AMOC [*Birgel and Hass*, 2004; *Hebbeln and Berner*, 1993] (Figure 1).

[3] Sediments in the Arctic basin are mainly derived from surrounding landmasses, and delivered as suspended particulate matter and bed loads from rivers and as wind-transported dust. In shallow margins, suspended particles are incorporated in sea ice during its formation and are transported over long distances throughout the Arctic Ocean [*Darby et al.*, 2006]. Pb isotopes in bulk sediment from deep-sea cores have proven to be useful tracers of the source areas for such detrital supplies [*Fagel et al.*, 2002, 2004; *Haley et al.*, 2008; *von Blanckenburg and Nägler*, 2001; *Winter et al.*, 1997]. In a complementary manner, the isotopic composition

[1]GEOTOP Research Center,Université du Québec à Montréal, Montréal, Quebec, Canada.
[2]Also at Centre de Recherches Pétrographiques et Géochimiques, CNRS/INSU, Vandoeuvre lès Nancy, France.
[3]TAKUVIK International Center for Arctic and Sub-Arctic Ecogeosystems Studies, CNRS, Centre d'études nordiques, Université Laval, Quebec, Quebec, Canada.
[4]Centre de Recherches Pétrographiques et Géochimiques, CNRS/INSU, Vandœuvre lès Nancy, France.

0883-8305/12/2011PA002152

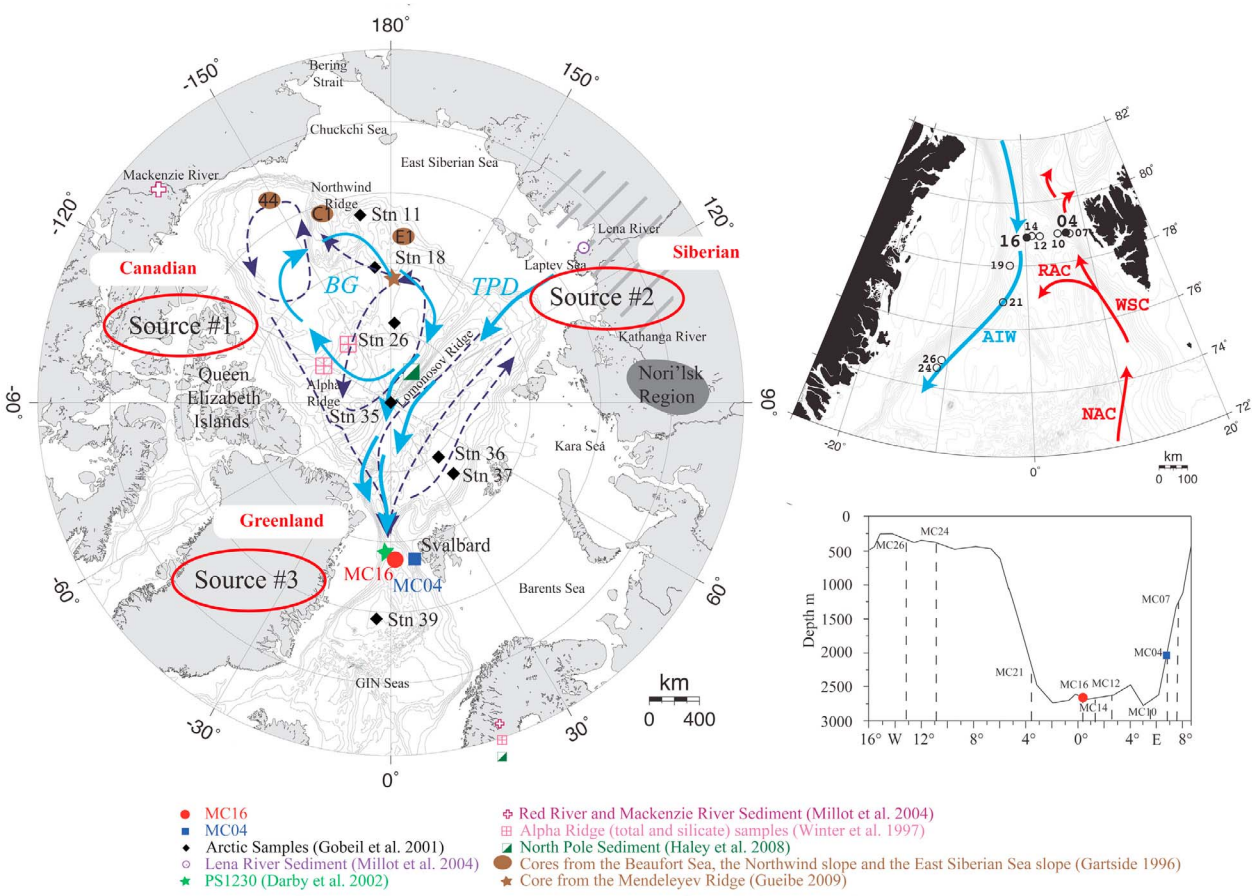

Figure 1. Bathymetric map of Fram Strait and surface sample locations. (left) Map of the Arctic Ocean. Light blue arrows represent main surface currents and dark blue dashed arrows represent deep currents. BG, Beaufort Gyre; TPD, Transpolar Drift [*Jones*, 2001; *Rudels et al.*, 2004, 2005]. (right, top) Open and solid circles represent surface and core samples along the transect, respectively. Red arrows illustrate warm Atlantic waters and blue arrows represent cold Arctic waters. NAC, North Atlantic Current; WSC, West Spitsbergen Current; RAC, Return Atlantic Current; AIW, Arctic Intermediate Waters. (right, bottom) Localization of surface samples versus water depth.

of Pb of exchangeable fractions leached from sediments (i.e., the authigenic sediment fraction) can be used to trace water mass circulation. This is facilitated by the short marine residence time of Pb in its dissolved form (<100 a) [*Henderson and Maier-Reimer*, 2002] which allows regional inputs to be identified. Whereas Pb isotopes are not fractionated by biological processes, recent studies have demonstrated that weathering processes can lead to some isotopic fractionation. Physically eroded rocks such as granitoids, in high latitudes, may preferentially release radiogenic Pb from damaged crystal structures [*Foster and Vance*, 2006; *Gutjahr et al.*, 2009; *Harlavan and Erel*, 2002; *Harlavan et al.*, 1998; *Kurzweil et al.*, 2010; *von Blanckenburg and Nägler*, 2001]. Thus the isotopic composition of exchangeable and dissolved Pb fractions derived from continental weathering could potentially differ from that of the detrital residue.

[4] Trace metals are precipitated from ambiant seawater onto sinking and sedimented particles by incorporation in authigenic Fe-Mn coatings. Such coatings have been studied in the western North Atlantic [*Gutjahr et al.*, 2009, 2008] and in the Arctic Ocean itself [*Haley et al.*, 2008] following the procedure developed by *Gutjahr et al.* [2007] to specifically leach this phase. The residual detritus left after the leaching procedure is thought to represent the pure terrigenous/detrital fraction of the sediment while leachates provide information concerning water masses.

[5] Here, we document changes in detrital supplies to marine sediments, mostly linked to Ice-Rafting Deposition (IRD), and variations in water mass geochemical properties that occurred since the Last Glacial Maximum (LGM). Our conclusions are based on Pb isotope data and a few trace element ratios, in residues and leachates from two sediment cores and surface sediments taken along a NE-SW transect across Fram Strait (Figure 1). In a preliminary study of these samples, *Carignan et al.* [2008] demonstrated that several elemental ratios (e.g., Th/U, Th/Zr) and Pb isotopes in bulk sedimentary fractions from the same area are sensitive tracers of changes in sources and trajectories of Fram Strait sediments. Previously, *Gobeil et al.* [2001] used Pb concentrations and isotopic compositions of surface sediments from several Arctic and sub-Arctic basins, to document anthropogenic Pb fluxes and sources. In this study, we use Th/Zr ratios of bulk sediments and residues as a first criterion for identifying the source components of the terrigenous fraction. In addition we use Pb isotopes

Table 1. Site Locations of Surface Samples

Sample Name	Water Depth (m)	Latitude	Longitude
BC07	1497	N 78° 52.620′	E 07° 20.459′
MC04	1181	N 78° 54.931′	E 06° 46.005′
BC10	2483	N 78° 56.176′	E 05° 24.075′
BC12	2426	N 78° 54.461′	E 02° 24.919′
BC14	2502	N 78° 55.888′	E 01° 06.460′
MC16	2546	N 78° 53.767′	E 01° 06.460′
MC21	1779	N 77° 00.204′	W 02° 30.173′
MC24	2974	N 74° 38.000′	W 03° 23.662′
MC26	3064	N 74° 53.490′	W 10° 46.100′

in leachates and residual sedimentary fractions to document particulate transport (sediment sources and trajectories) and exchange with carrier water masses, as well as mixing processes in surface sediment. The time frames of the two sediment cores, MC04 and MC16, encompass the very late Holocene and the LGM present interval, respectively, and thus provide time resolution varying from the centennial to the millennial scale. We particularly concentrate our efforts on core MC16, both because this core provides a record since the LGM and because it is composed primarily of ice-rafted detritus, thus allowing reconstruction of sea ice and water mass exports from the Arctic into the northern North Atlantic over the past ~20 ka.

2. Materials and Methods

2.1. Sampling Sites and Settings

[6] The sediment cores were collected during the 2006 *WarmPast* Cruise on the R/V JanMayen along a NE-SW transect across Fram Strait [*Husum*, 2006]. Ten sites (Figure 1 and Table 1) provided material that can be used to document modern particulate sources and trajectories. Here, we examine surface samples obtained from eight of these sites using box cores or multicores, as well as two long (40–50 cm) multicores, JM06-WP-04-MC (MC04) and JM06-WP-16-MC (MC16). MC04 was taken in the east, below the NAW incoming from the Greenland, Icelandic and Norwegian (GIN) seas, whereas MC16 was taken in the west, below the outflowing Arctic waters (Figure 1) [*Dickson et al.*, 2007; *Husum*, 2006]. These cores were subsampled at 1 cm intervals onboard the JanMayen. Core MC04 illustrates conditions below the West Spitsbergen Current (WSC) that enters the Arctic basin through the eastern Fram Strait area. Core MC16 is under the influence of cold Arctic waters and sea ice flowing south. The outflowing water masses are 1) at the surface, the Modified Atlantic Water (MAW); 2) in the upper subsurface, the Arctic Atlantic Water; (AAW), 3) at greater depths, the Arctic Intermediate Water (AIW); and 4) at the seafloor, the Canadian Basin Deep Water (CBDW) and Eurasian Basin Deep Water (EBDW), which eventually merge into the North Atlantic Deep Water (NADW) [*Fahrbach et al.*, 2001; *Jones*, 2001; *Rudels et al.*, 2005; *Rudels et al.*, 2000].

2.2. Age Model

[7] All ages will be presented in calibrated years BP. The age models used for establishing the chronology of the two cores are based primarily on radiocarbon ages calibrated using the Calib 6.0 curve [*Reimer et al.*, 2009]. In the absence of a consensus regarding reservoir ages within the Arctic, no reservoir age has been added to the MARINE09 calibration (ΔR of 0). MC04 chronology is based on ^{14}C dating of planktonic foraminifera assemblages (see *Bonnet et al.*, [2010] for more details). Core MC04 (~2.5 ka present) displays a mean sedimentation rate of ~18 cm/ka. Site MC04 is influenced by productive Atlantic waters [*Dokken and Hald*, 1996; *Hebbeln et al.*, 1994] and hence has a relatively high microfossil accumulation rate.

[8] Site MC16 is influenced by Arctic waters and remains ice covered almost all year long [*Elverhøi et al.*, 1998; *Hebbeln*, 2000]. As a result, most of the sediment is derived from ice-rafting processes and sedimentation rates are much lower than those of core MC04. The age model established for site MC16 is based on three ^{14}C measurements from three planktonic foraminifera assemblages [*Zamelczyk et al.*, 2010], a tephrochronological date [*Zamelczyk et al.*, 2010] and correlations with cores (MC-18 and TC-18) from the Lomonosov Ridge [*Hanslik et al.*, 2010; C. Not and C. Hillaire-Marcel, A trigger from the Arctic: The most plausible scenario for the Younger Dryas cold spell, submitted to *Nature Communications*, 2011]. Cores MC-18 and TC-18, located in an intrabasin of the Lomonosov Ridge, are upstream of core MC16, on the pathway of the merging Beaufort Gyre and Trans-Polar Drift (Figure 1). MC-18 revealed a fivefold higher sedimentation rate during the Younger Dryas (YD; ~12–13 ka), compared to the mean Holocene rate, that Not and Hillaire-Marcel (submitted manuscript, 2011) ascribed to enhanced sea ice drifting along the Beaufort Gyre which deposited detrital material carrying a strong NW Canadian margin (Mackenzie River area) mineralogical signature.

[9] In core MC16, ash grains found at 16 cm were tentatively identified as belonging to the Vedde Ash event on the basis of their geochemical characteristics. This ash deposit has been dated elsewhere at ~12.1 calibrated (cal.) ka [*Thornalley et al.*, 2011, and references therein] and thus falls near the end of the YD event. Slightly lower in the core, at a depth of 20 cm, Pb isotopes display a strong excursion toward compositions similar to that of the Mackenzie River indicating a Canadian margin source area (see below). The onset of the YD has been assigned to this excursion, which we correlate to that observed in the Lomonosov Ridge, though we recognize some circularity in this reasoning.

[10] The age model retained for MC16 (Figure 2) suggests a mean sedimentation rate of 2.3 cm/ka below 20 cm, i.e., for the LGM early deglacial interval. The sedimentation rate increased to about 5 cm/ka from 20 to 14 cm, during the YD event itself. Finally, during the Holocene, it has decreased to a mean value of ~1.1 cm/ka. Unfortunately, this poorly constrained age model does not allow us to identify potential intervals of hiatus or short-term changes in sedimentation rates. However, it suggests similar ~5 fold higher sedimentation rates during the YD, compared to the Holocene, as estimated by Not and Hillaire-Marcel (submitted manuscript), upstream on the IRD route, in the Lomonosov Ridge area.

2.3. Analytical Methods

2.3.1. ^{210}Pb and ^{137}Cs Measurements

[11] Bulk fractions from sediment samples were used for ^{210}Pb and ^{137}Cs measurements (Table 2 and auxiliary material),

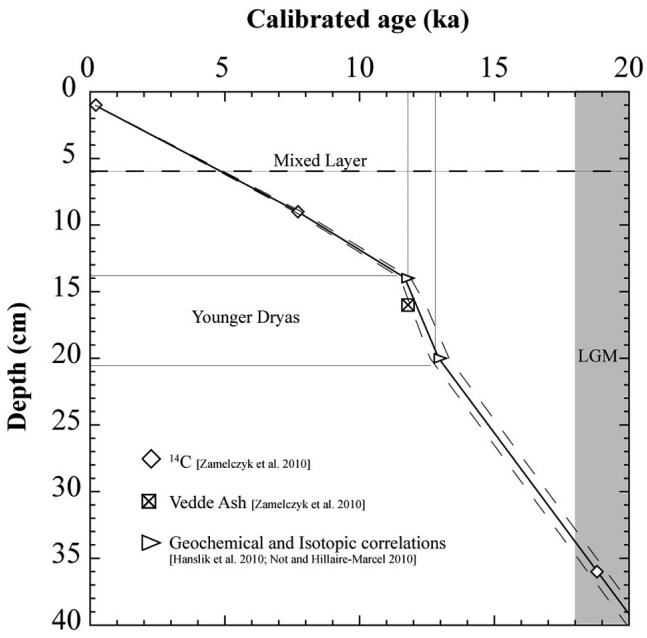

Figure 2. Age model of depth versus calibrated age for core MC16 using ^{14}C dates, tephrochronological layer identification, and geochemical correlations with nearby sediment cores. Dashed lines above and below the age model curve represent the estimated uncertainty. The mixed layer, down to 6 cm, is represented by a dashed line.

in order to document mixing processes in surface sediments.[1] Pb isotopes in modern sediments (Table 3) carry an anthropogenic signature [*Gobeil et al.*, 2001] and, along with ^{210}Pb and ^{137}Cs measurements, allow assessment of the maximum depth of anthropogenic inputs in the sediment and hence help define the mixed layer. Sediment subsamples were dried and ground. ^{210}Pb activities were determined by measuring the radioactive decay of its daughter isotope ^{210}Po ($t_{1/2}$ = 138.4 days; α = 5.30 MeV) by alpha spectrometry [*Ghaleb*, 2009]. A ^{209}Po spike was added as a yield and counting efficiency tracer. Po was extracted and purified by chemical treatment and deposited on silver disks following the method of *Flynn* [1968]. The ^{209}Po and ^{210}Po activities were measured in a silicon surface barrier α spectrometer (EGG and ORTEC type 576A). ^{137}Cs was measured by γ spectrometry at 66.6 keV, using a low background high-purity Ge well detector (Canberra). IAEA-300 standard reference material was used as a counting efficiency tracer of the detector and to estimate the reproductibility (1σ = 1%).

2.3.2. Separation of Authigenic and Residual Components

[12] Bulk sediments are composed of distinct fractions: 1) exchangeable, 2) bound to carbonates, 3) bound to Fe-Mn oxides, 4) bound to organic matter, and 5) the residual detrital fraction [*Bayon et al.*, 2002; *Gutjahr et al.*, 2007; *Tessier et al.*, 1979]. Fe-Mn oxides are leachable phases that are thought to precipitate either during settling of particles within the water column or at the sediment/water interface, incorporating trace metals directly from the water masses. The leachable fractions may thus record properties of overlying deep-water masses, but may also include some soluble/exchangeable elements hosted by detritic phases (e.g., exchangeable metals in clay). Thus it is important to choose a leaching technique that releases "authigenic" fractions, i.e., that exchanged with or formed directly from dissolved fractions in overlying water masses. However, it is necessary to first remove the carbonate fraction, as it may have a mixed detrital-authigenic origin. The methodology we have chosen is based mostly upon techniques developed by *Bayon et al.* [2002] and *Gutjahr et al.* [2007]. Sediments are first sieved through a nylon mesh with milli-Q™ water to obtain fractions with grain sizes <100 μm. As nearly all of the sediment is in this size range, this step serves to remove stray, unrepresentative large grains. After drying and grinding, aliquots of ca. 300 mg are accurately weighed in Teflon™ beakers. Weighing and all subsequent chemical treatment were performed in a class 100 clean lab. Carbonates are removed by adding 1 2 mL of a Na acetate buffer (1M, Acetic acid 1M; 52:48) and shaking at room temperature for 3 h. Samples are centrifuged and the supernatant, containing the carbonate fraction, is removed. Residues are rinsed three times with milli-Q™ water, then subjected to repeated centrifugation (typically 3 times), dried, weighed and ground in an agate mortar. 12 mL of a solution of 0.05 M Hydroxylamine Hydrochloride (HH), 15% acetic acid, 0.03 M Na-EDTA, buffered to pH 4 with analytical grade NaOH, is added to the residue and shaken at room temperature for 24 h. The supernatant, which will henceforth be referred to as the leachate, is recovered, and residues are rinsed as previously described and the rinse water is added to the supernatant. The leachate obtained from this procedure is dominated by the Fe-Mn oxyhydroxyde fraction, but we cannot exclude the possibility of a minor contribution from other phases.

2.3.3. Major and Trace Element Analyses

[13] All subsequent analyses were performed on the <100 μm aliquot fractions. After sieving, sediment samples were dried and ground in an agate mortar. The bulk sediment powders, as well as leachates and residues obtained after carbonate and Fe-Mn oxide removal, were analyzed for major and trace elements at the Service d'Analyse des Roches et Minéraux (SARM-CNRS), Nancy, France, following procedures described by *Carignan et al.* [2008, and references therein]. Calibration curves and accuracy controls were performed using international geological reference materials. Total concentration uncertainties were about 1% for major elements and between 5% and 10% for trace elements, depending on concentration levels.

Table 2. ^{210}Pb and ^{137}Cs Activity Data From the Bulk Sediment From Core MC16

Sample Depth (cm)	^{210}Pb Activity (dpm/g)	^{137}Cs (dpm/g)
0–1	29.34	0.38
1–2	24.86	0.39
2–3	11.42	0.26
3–4	8.21	0.13
4–5	4.91	-
5–6	3.08	-
6–7	2.61	-
7–8	2.47	-
8–9	2.44	-
9–10	2.49	-

[1]Auxiliary materials are available in the HTML. doi:10.1029/2011PA002152.

Table 3. Elemental and Pb Isotopic Data From Total, Detrital, and Leachable Fractions From MC16[a]

		Total				Residues							Leachates						
Interval Depth (cm)	Age (calibrated Ka)	Al_{tot} (%)	Zr_{tot} (μg/g)	Th_{tot} (μg/g)	Pb_{tot} (μg/g)	Al (%)	Zr (μg/g)	Th (μg/g)	Pb (μg/g)	$^{206}Pb/^{204}Pb$	$^{207}Pb/^{204}Pb$	$^{208}Pb/^{204}Pb$	Al (%)	Th (μg/g)	Pb (μg/g)	Removed Pb (%)	$^{206}Pb/^{204}Pb$	$^{207}Pb/^{204}Pb$	$^{208}Pb/^{204}Pb$
0–1	0.2	7.0	137.9	7.3	28.0	6.3	152.5	5.3	7.4	18.633	15.601	38.628	0/96	2.3	25.2	77	18.472	15.608	38.403
1–2	1.1	6.9	161.3	7.8	39.8	6.7	182.9	6.5	7.9	18.674	15.596	38.804	0.111	2.1	30.6	79	18.331	15.610	38.288
2–3	2.0	6.9	148.9	7.0	25.3	6.7	185.9	6.2	7.5	18.660	15.594	38.773	0.107	1.9	18.9	72	18.503	15.620	38.485
3–4	2.9	7.0	202.7	9.3	35.9	6.4	151.6	5.6	7.5	18.684	15.588	38.871	0.095	2.4	26.4	78	18.338	15.601	38.298
4–5	3.8	7.4	160.1	7.5	21.7	6.9	192.9	6.1	7.5	18.701	15.602	38.719	0.104	2.4	13.9	65	18.608	15.608	38.573
5–6	4.7	7.3	201.0	9.9	30.2	6.9	186.6	5.8	7.1	18.621	15.592	38.771	0.157	2.0	17.3	71	18.442	15.608	38.405
6–7	5.6	7.4	206.9	10.2	20.5	7.1	182.0	6.2	7.1	18.711	15.608	38.863	0.128	2.2	11.5	62	18.787	15.630	38.771
7–8	6.5	7.3	216.0	10.3	22.0	6.8	199.5	6.5	7.6	18.680	15.592	38.751	0.196	2.9	13.7	64	18.709	15.632	38.701
8–9	7.5	7.2	224.9	9.9	23.6	6.7	215.7	6.8	8.0	18.655	15.592	38.871	0.243	2.5	14.7	65	18.593	15.629	38.589
9–10	8.3	7.4	186.0	7.8	22.2	6.9	209.8	6.7	8.0	18.714	15.598	38.785	0.094	2.8	15.1	66	18.584	15.613	383545
10–11	9.2	7.3	205.0	10.2	27.4	-	-	-	-	-	-	-	-	-	-	-	-	-	-
11–12	10.0	7.5	188.9	10.3	28.2	-	-	-	-	-	-	-	-	-	-	-	-	-	-
12–13	10.9	7.6	189.9	10.7	28.8	-	-	-	-	-	-	-	-	-	-	-	-	-	-
13–14	11.8	7.8	191.7	11.3	28.2	-	-	-	-	-	-	-	-	-	-	-	-	-	-
14–15	12.0	8.0	205.0	10.2	26.6	7.3	189.8	7.0	7.7	18.733	15.601	38.832	0.238	2.8	15.7	64	18.624	15.620	38.589
15–16	12.2	8.3	208.0	10.7	30.6	-	-	-	-	-	-	-	-	-	-	-	-	-	-
16–17	12.4	8.1	221.6	11.1	26.4	-	-	-	-	-	-	-	-	-	-	-	-	-	-
17–18	12.6	8.0	236.1	10.6	23.7	-	-	-	-	-	-	-	-	-	-	-	-	-	-
18–19	12.8	8.0	231.3	11.0	26.5	-	-	-	-	-	-	-	-	-	-	-	-	-	-
19–20[b]	13.0	8.3	188.9	10.3	21.8	8.0	181.1	7.7	8.0	**18.836 ± 0.019**	**15.6178 ± 0.0003**	**38.831 ± 0.054**	0.068	2.7	12.3	60	18.831	15.632	38.771
21–22	13.9	8.3	189.9	10.7	29.8	7.6	204.4	6.4	7.9	18.684	15.599	38.688	0.120	3.2	18.7	69	18.569	15.623	38.516
22–23	14.3	8.3	191.7	11.3	25.1	7.6	221.2	6.8	8.1	18.695	15.593	38.824	0.117	3.4	17.0	66	18.647	15.626	38.599
24–25[c]	15.1	7.8	**225 ± 35**	**10.1 ± 0.7**	**18.9**	-	-	-	-	**18.65 ± 0.07**	**15.589 ± 0.008**	**38.64 ± 0.11**	-	-	-	-	17.621	15.562	37.532
26–27[c]	16.0	8.2	**228.1 ± 3.3**	**8.8 ± 0.1**	**24.9**	**7.5**	211.6	6.4	7.7	**18.611 ± 0.069**	**15.587 ± 0.017**	**38.606 ± 0.042**	0.154	3.0	16.5	66	18.558	15.618	38.523
27–28	16.4	8.0	221.6	11.1	23.0	7.4	202.0	5.2	6.6	18.589	15.581	38.569	0.118	3.0	15.5	68	18.579	15.616	38.547
29–30[c]	17.3	8.2	**189 ± 13**	**9.1 ± 1.3**	**19.2**	7.4	199.2	6.1	6.5	**18.666 ± 0.016**	**15.598 ± 0.002**	**38.650 ± 0.022**	0.103	3.4	12.9	64	18.728	15.620	38.750
34–35[c]	19.4	8.2	**219.9 ± 5.2**	**10.0 ± 0.5**	**20.4**	**7.6**	221.6	7.0	9.1	**18.708 ± 0.057**	**15.603 ± 0.009**	**38.696 ± 0.040**	0.126	2.8	11.4	58	18.764	15.630	38.794
35–36[c]	19.8	7.7	**224 ± 35**	**10.0 ± 0.1**	**20.0**	**7.2**	217.1	5.6	7.6	**18.469 ± 0.093**	**15.573 ± 0.009**	**38.45 ± 0.18**	0.012	2.2	9.4	54	18.592	15.618	38.576
36–37	20.2	8.1	210	10.6	21.4	7.7	185.0	5.6	7.7	18.598	15.590	38.621	0.136	3.2	17.0	68	18.537	15.620	38.523
37–38[c]	20.7	7.6	**234 ± 21**	**9.2 ± 0.3**	**17.8**	-	-	-	-	**18.75 ± 0.13**	**15.608 ± 0.016**	**38.806 ± 0.057**	-	-	-	-	17.953	15.579	37.872
39–40[b]	21.5	7.8	174.2	7.9	17.7	7.3	230.8	6.7	8.3	**18.661 ± 0.021**	**15.599 ± 0.012**	**38.623 ± 0.025**	0.099	2.9	10.3	74	18.770	15.618	38.742

[a]Leachate concentrations are reported relative to the initial bulk sediment mass. Bold values represent the mean and standard deviation of repeated analyses, while the other values represent the value obtained from a single analysis.

[b]Isotopic values correspond to the mean of duplicate analyses of the same leached aliquot fraction.

[c]Isotopic values correspond to the mean of analyses of leached aliquot fractions from different subsamples at the same level.

2.3.4. Pb Isotopic Analyses

[14] Pb isotopic analyses were performed on residues of the sieved (<100 μm) sediment after carbonate and Fe-Mn oxide removal, as well as on the leachates thought to represent the Fe-Mn oxide fraction. In this respect, they differ from the Pb analyses presented in the preliminary study of *Carignan et al.* [2008], which were performed on bulk sediment powders. For the residues, approximately 100 mg of powder were weighed and digested with a mixture of HF, HNO_3 and HCl on a hot plate at 110°C. This acid mixture was also added to the leachates, after partial evaporation, to ensure dissolution of any precipitates. Pb was extracted using anion exchange chromatography, following *Manhes et al.* [1980]. Measurements were performed on a (MC)-ICP-MS Isoprobe™, at either the CRPG laboratory in Nancy, France or the GEOTOP laboratory in Montreal, Canada. In both cases, the standard reference material NIST 981 was used as a reference. Instrumental mass bias was corrected internally after addition of SRM NIST 997 Tl solution [*White et al.*, 2000]. Nominal isotopic values used for Pb and Tl ($^{205}Tl/^{203}Tl$ of 2.3889) reference materials were taken from *Thirlwall* [2002]. Analytical uncertainty was estimated by repeated measurement of the Pb-Tl reference material. Calculated NIST 981 Pb ratios indicate an overall reproducibility better than 150 ppm/amu (2*sd of the mean: $^{208}Pb/^{206}Pb$: 2.43380 ± 0.00029; $^{206}Pb/^{207}Pb$: 1.09308 ± 0.00012; $^{207}Pb/^{206}Pb$: 0.91485 ± 0.00017; $^{208}Pb/^{204}Pb$: 36.722 ± 0.011; $^{207}Pb/^{204}Pb$: 15.4974 ± 0.0047; $^{206}Pb/^{204}Pb$: 16.9398 ± 0.0053). Blanks for the Pb procedure in detrital residues were under 0.9 ng and represent less than 0.30% of the total amount of Pb present in the samples. Blanks for the leachate fraction represent less than 0.46% of the total Pb present.

2.4. Sediment Sample Heterogeneity

[15] Before discussing the results, we address the methodological issue of the representativity/heterogeneity of glacial sediment subsamples. As illustrated in Table 4, some variability is observed, not only with varying depth, but even between distinct ~1 cc subsamples taken from a single 1 cm thick core slice. Two explanations can be suggested. The first is procedural. We can rule out biases in the mass spectrometric measurements, since analyses of the same homogenized residue powder performed in the two laboratories yield identical results within standard deviation (Table 4, samples at 19–20 cm and 39–40 cm). Incomplete digestion of certain heavy minerals could also potentially influence the measured isotopic compositions. However, the reproducibility of replicates of the same leached subsamples in different laboratories also argues against this possibility. On the other hand, since different subsamples were sieved and leached in different laboratories, we cannot exclude the possibility of small biases due to subtle procedural differences, particularly in the leaching technique, despite our efforts to use identical techniques. A more likely explanation from our point of view is that the sediments are intrinsically heterogeneous at the sampling level. All of our analyses of duplicate subsamples are from the glacial to late glacial interval. This time period is marked by large Pb isotopic heterogeneities linked to a rapidly changing sedimentary regime (see below). Therefore, 1 cm^3 of material that corresponds to several hundred years may not be representative of the mean sedimentary properties of the corresponding layer. To get around this issue, in the discussion we use mean values from available measurements for a given layer, and underscore the statistical uncertainties inherent in this type of sampling.

3. Results

3.1. ^{137}Cs and ^{210}Pb Abundances: Definition of the Mixed Layer

[16] Previous ^{210}Pb and ^{137}Cs analyses of sediments from core MC04 suggested a thickness of about 10 cm for the modern mixed layer (see *Bonnet et al.* [2010] for more details). In core MC16, elevated ^{137}Cs levels extend down to at least the 3–4 cm interval, while above background levels of ^{210}Pb are found to around 6–7 cm (Table 2 and auxiliary material). This indicates that the modern mixed layer in this core is about 6 cm thick. This value is unlikely to represent mixing conditions in the past, especially prior to the Holocene, because primary productivity and benthic mixing were reduced [*Zamelczyk et al.*, 2010]. In particular, foraminiferal abundance presents very sharp peaks (with a significant increase in number) deeper in the core, suggesting that bioturbation was less intense in the past.

3.2. The Pb Budget in the Sediment Cores

[17] Figure 3 presents both bulk and residue Pb/Al ratio profiles in cores MC04 (Figure 3a and Table 5) and MC16 (Figure 3b and Table 3). Pb/Al ratios, rather than absolute Pb concentrations are compared because absolute concentrations in bulk samples can be affected by dilution by carbonates. Aluminum was chosen as the normalizing element for several reasons. Al is an immobile element, as shown by the fact that less than 2% is removed during the leaching procedure. Al is derived from terrigenous inputs and represents alumino silicates, the main group of minerals found in fine sediment fractions. Anthropogenic inputs of Al are negligible. Al is also nonreactive, thus its levels will not change as a consequence of chemical reactions within the sediment [*Fütterer*, 2000]. In addition, Al is a major element and thus does not usually display the 'nugget' effects frequently observed for crustal trace elements. Al is hence an excellent choice when normalizing for terrigenous inputs. Comparison of Pb/Al ratios of the bulk and residual fractions allows us to constrain the relative importance of the various components of the Pb budget (detrital, leachable geogenic and leachable anthropogenic).

[18] In both cores, Pb/Al ratios in residual fractions remain nearly constant with depth. In contrast, Pb/Al ratios of the bulk sediment are significantly higher throughout the profiles, and increase markedly in the mixed layers, most probably because of the addition of Pb of anthropogenic origin. In accordance with this observation, common Pb concentrations in leachates of the upper 6–7 cm of core MC16 are higher than those from deeper in the core (Table 3), thus confirming the above estimate of the mixed layer thickness from ^{210}Pb abundances. Based on the quantities of Pb in the bulk, residual and leachate fractions, we estimate that 59 ± 4% and 65 ± 5% of the Pb is removed during the leaching procedure in samples from below the mixed layer in cores MCO4 and MC16, respectively. (These percentages correspond to the proportion of Pb removed during the final leaching step relative to the total amount of Pb in the decarbonated sediment.) In the mixed layer these proportions increase to 84 ± 3% and

Table 4. Elemental and Pb Isotopic Data From Total, Detrital, and Leachable Fractions from Duplicate Samples From Core MC16[a]

		Total			Residues						Leachates					
Interval Depth (cm)	Age (calibrated Ka)	Zr_{tot} (μg/g)	Th_{tot} (μg/g)	Pb_{tot} (μg/g)	Zr (μg/g)	Th (μg/g)	Pb (μg/g)	$^{206}Pb/^{204}Pb$	$^{207}Pb/^{204}Pb$	$^{208}Pb/^{204}Pb$	Th (μg/g)	Pb (μg/g)	Removed Pb (%)	$^{206}Pb/^{204}Pb$	$^{207}Pb/^{204}Pb$	$^{208}Pb/^{204}Pb$
19–20 Mean[b] ± 1*sigma	13.0	188.9	10.3	21.8	181.1	7.7	8.0	18.823	15.618	38.869	2.7	12.3	60	18.831	15.632	38.771
								18.850	15.618	38.793						
								18.836 ± 0.019	**15.6178 ± 0.0003**	**38.831 ± 0.054**						
24–25 Mean ± 1*sigma	15.1	200.3	10.6	47.6	-	-	-	18.236[c]	15.562[c]	38.297[c]	-	-	-	17.621[c]	15.562[c]	37.532[c]
		-	-	-				18.696	15.595	38.713				-	-	-
		249.2	9.6	18.9				18.597	15.584	38.636				18.733	15.612	38.676
		225 ± 35	**10.1 ± 0.7**	18.9				**18.65 ± 0.07**	**15.589 ± 0.008**	**38.64 ± 0.11**				**18.733**	**15.612**	**38.676**
26–27 Mean ± 1*sigma	16.0	230.4	8.9	24.9	211.6	6.4	7.7	18.562	15.578	38.577	3.0	16.5	66	18.558	15.618	38.523
		225.7	8.7	17.5				18.659	15.596	38.636				18.757	15 .604	38.681
		228.1 ± 3.3	**8.8 ± 0.1**	**21.2 ± 5.2**				**18.611 ± 0.069**	**15.587 ± 0.017**	**38.606 ± 0.042**				**18.657 ± 0.14**	**15.611 ± 0.009**	**38.602 ± 0.11**
29–30 Mean ± 1*sigma	17.3	198.5	10.0	19.2	199.2	6.1	6.5	18.677	15.597	38.666	3.4	12.9	64	18.728	15.620	38.750
		179.3	8.2	19.6				18.655	15.3600	38.634				18.724	15.613	38.719
		189 ± 13	**9.1 ± 1.3**	**19.4 ± 0.3**				**18.666 ± 0.016**	**15.598 ± 0.002**	**38.650 ± 0.022**				**18.726 ± 0.003**	**15.616 ± 0.005**	**38.735 ± 0.02**
34–35 Mean ±1*sigma	19.4	223.6	9.6	20.4	221.6	7.0	9.1	18.668	15.596	38.667	2.8	11.4	58	18.764	15.630	38.794
		216.2	10.4	19.4				18.749	15.609	38.724				18.724	15.610	38.697
		219.9 ± 5.2	**10.0 ± 0.5**	**19.9 ± 0.8**				**18.708 ± 0.057**	**15.603 ± 0.009**	**38.696 ± 0.040**				**18.744** ± 0.028	**15.620 ± 0.14**	**38.746 ± 0.07**
35–36 Mean ±1*sigma	19.8	198.5	10.0	20.0	217.1	5.6	7.6	18.536	15.579	38.580	2.2	9.4	54	18.592	15.618	38.576
		249.2	10.1	18.2				18.404	15.566	38.323				18.608	15.609	38.560
		224 ± 35	**10.0 ± 0.1**	**19.1 ± 1.3**				**18.469 ± 0.093**	**15.573 ± 0.009**	**38.45 ± 0.18**				**18.600** ± 0.011	**15.613 ± 0.006**	**38.568 ± 0.11**
37–38 Mean ±1*sigma	20.7	248.4	9.0	42.4	-	-	-	18.027[c]	15.553[c]	37.927[c]	-	-	-	17.953[c]	15.579[c]	37.872[c]
		218.8	9.5	17.8				18.657	15.596	38.766				18.676	15.601	38.620
				17.8				18.841	15.619	38.846				18.714	15.605	38.658
		234 ± 21	**9.2 ± 0.3**					**18.75 ± 0.13**	**15.608 ± 0.016**	**38.806 ± 0.057**				**18.695 ± 0.03**	**15.605 ± 0.0004**	**38.639 ± 0.03**
39–40 Mean[c] ± 1*sigma	21.5	174.2	7.9	17.7	230.8	6.7	8.3	18.647	15.590	38.606	2.9	10.3	11.1	18.770	15.618	38.742
								18.676	15.607	38.641						
								18.661 ± 0.021	**15.599 ± 0.012**	**38.623 ± 0.025**						

[a]Leachate concentrations are reported relative to the initial bulk sediment mass. Bold values represent the mean and standard deviation of repeated analyses, while the other values represent the value obtained from a single analysis.

[b]Analyses were performed on the same leached aliquot fraction. (All other duplicate analyses were performed on leached aliquots from different subsamples of the same level.)

[c]The first set of values of samples at 25 and 38 cm have been rejected due to enhanced concentrations of Pb in the bulk sediments that we have interpreted as a possible contamination effect. The means have been calculated using the two subsequent values.

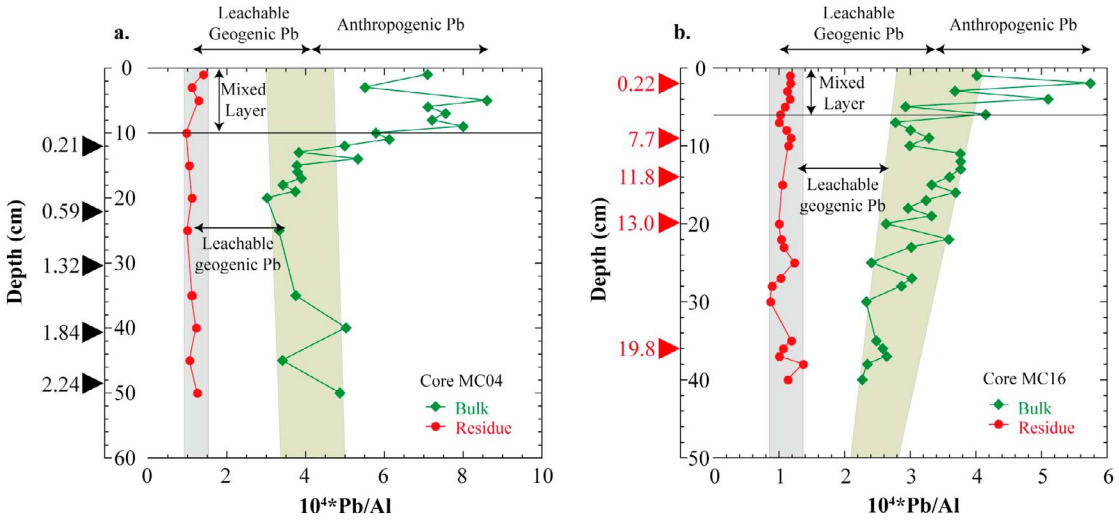

Figure 3. Pb/Al ratios in the bulk sediment (green diamonds) and in the detrital residue (red circles) illustrating the Pb budget in (a) core MC04 and (b) core MC16. Grey fields represent the crustal, nonleachable Pb. Green fields represent the geogenic Pb determined from the bulk sediments and include all values below the mixed layer defined by ^{137}Cs and ^{210}Pb data. The difference between the gray and green fields represents the leachable geogenic Pb. Pb concentrations were measured on more bulk samples than on residues; hence all bulk samples do not have a corresponding residue. Specific calibrated ages (in ka) are indicated by arrows on the depth axes.

74 ± 5%. On average, the leaching procedure thus removed 42% (MC04) and 14% (MC16) more Pb in the mixed layer than in the rest of the core. This excess Pb probably represents the anthropogenic contribution (Figure 3), larger in core MC04 than in MC16. The bulk fractions of the surface samples are thus imprinted by anthropogenic Pb inputs [*Gobeil et al.*, 2001]. Pb concentrations in residual fractions show little difference between samples from the mixed layer and those from deeper sediments. We conclude that the leachable Pb, including anthropogenic Pb, has been efficiently removed during the leaching procedure.

[19] The Pb contained in the fraction removed by Na acetate leaching is thought to represent the Pb contribution from carbonates. While the Pb content of this fraction was not directly measured, it has been estimated by calculating the difference between bulk sample Pb content and the sum of the Pb contents recovered in 1) leachates (from the HH acetic acid-EDTA leaching step) and 2) residues. In the mixed layer of MC04, almost no Pb was removed by the Na acetate leachates whereas in deeper sediment, an average of 30% of Pb was apparently removed. However, due to minor losses during each step of the analytical procedure, the missing 30% should be seen as a maximum value for the Pb hosted by carbonates. For comparison, in core MC16, an average of 1% was removed by the Na acetate solution in mixed layer samples, whereas an average of 3% was removed downcore. Due to potential losses mentioned above along with a 10% uncertainty on the analysis itself, this difference may be seen as insignificant.

3.3. Surface Sediments

[20] Elemental ratios and Pb isotopes from the surface samples of the transect (Figure 1) are plotted versus longitude in Figure 4 and corresponding data are listed in Table 6. Th/Zr ratios depend almost entirely on detrital silicate supplies and provide a first criterion for discriminating potential sources. This ratio can be used to define at least three distinct sedimentary fields in the Fram Strait area. The easternmost field, on the west Spitsbergen shelf (core MC07, Figure 4), displays a Th/Zr value of 0.031. Off the Spitsbergen margin, below the WSC, values ranging from 0.041 to 0.045 are observed. Westward, off the Greenland margin, mostly under the influence of outflowing Arctic water masses and sea ice, Th/Zr ratios return to lower values (0.035 to 0.028).

[21] Total Th/Pb ratios in surface sediments are influenced by anthropogenic Pb contamination [*Carignan et al.*, 2008; *Gobeil et al.*, 2001]. Th/Pb ratios in the bulk sediment of the surface samples, which contain both natural and anthropogenic Pb, show only limited variability along the transect. In contrast, Th/Pb ratios of residual fractions vary geographically in a manner similar to that of Th/Zr ratios. Residual Th/Pb values of 0.72, 0.81–0.91, and 0.71–0.75 are obtained for each of the sedimentary fields identified above, along the NE to SW transect. This confirms that the detrital Pb fraction can also be used to discriminate between sediment sources [*Fagel et al.*, 2004, and references therein]. This is further demonstrated by distinct Pb isotope signatures in this fraction, with ^{206}Pb/^{204}Pb ratios of ~18.650, 18.744 to 18.837 and ~18.554, over the Sptisbergen Shelf, off the Spitsbergen margin, and along the Greenland margin.

3.4. Sedimentary Time Series

[22] In the long cores, residual Th/Zr and ^{206}Pb/^{204}Pb ratios vary with depth within the ranges of 0.038–0.49 and 18.650–18.958 (MC04, Figure 5 and Table 5) and 0.026–0.042 and 18.404–18.823 (MC16, Figure 5 and Table 3). The two cores display different Late Holocene values for these ratios in samples taken just below the mixed layer. Further back in time (LGM to Late Holocene), in the MC16

Table 5. Elemental and Pb Isotopic Data From Total, Detrital, and Leachable Fractions From MC04[a]

	Total				Residues							Leachates						
Interval Depth (cm)	Al_{tot} (%)	Zr_{tot} (μg/g)	Th_{tot} (μg/g)	Pb_{tot} (μg/g)	Al (%)	Zr (μg/g)	Th (μg/g)	Pb (μg/g)	$^{206}Pb/^{204}Pb$	$^{207}Pb/^{204}Pb$	$^{208}Pb/^{204}Pb$	Al (μg/g)	Th (μg/g)	Pb (μg/g)	Removed Pb (%)	$^{206}Pb/^{204}Pb$	$^{207}Pb/^{204}Pb$	$^{208}Pb/^{204}Pb$
0–1	6.1	144.1	7.6	43.1	6.8	130.7	5.3	7.8	18.650	15.583	38.554	99	1.8	31.4	80	18.262	15.576	38.128
2–3	6.8	130.2	7.1	37.5	8.1	134.4	5.5	6.8	18.835	15.621	38.736	117	2.2	32.9	83	18.407	15.613	38.303
4–5	6.8	146.0	9.4	58.7	8.3	122.2	6.0	8.0	18.835	15.616	38.755	141	2.4	48.3	86	18.275	15.604	38.193
5–6	6.9	141.2	9.4	49.0	-	-	-	-	-	-	-	-	-	-	-	-	-	-
6–7	6.9	154.7	9.6	51.8	-	-	-	-	-	-	-	-	-	-	-	-	-	-
7–8	6.9	163.8	9.8	50.0	-	-	-	-	-	-	-	-	-	-	-	-	-	-
8–9	6.8	165.5	9.6	54.3	-	-	-	-	-	-	-	-	-	-	-	-	-	-
9–0	6.7	131.6	7.3	39.0	8.1	127.9	5.3	5.8	18.958	15.638	38.886	136	2.3	37.1	86	18.498	15.620	38.444
10–11	6.8	165.0	9.9	41.6		-	-	-	-	-	-	-	-	-	-	-	-	-
11–12	6.8	165.8	9.5	33.8		-	-	-	-	-	-	-	-	-	-	-	-	-
12–13	6.9	167.0	9.7	26.5		-	-	-	-	-	-	-	-	-	-	-	-	-
13–14	7.0	173.1	10.1	37.2		-	-	-	-	-	-	-	-	-	-	-	-	-
14–15	7.0	182.3	9.9	26.4	8.1	195.1	7.5	8.4	18.924	15.633	38.815	1	1.9	11.9	58	18.655	15.635	38.597
19–20	7.1	136.7	7.6	21.6	8.3	141.8	6.0	7.6	18.660	15.594	38.773	218	2.3	9.7	56	18.709	15.626	38.626
24–25	7.0	173.2	10.1	23.3	8.2	191.5	7.6	8.2	18.956	15.632	38.829	2	2.3	9.7	54	18.792	15.649	38.734
34–35a	7.1	176.0	9.9	26.6	7.9	144.9	6.1	7.1	18.926	15.627	38.867	165	2.5	10.2	59	18.572	15.604	38.474
34–35b	7.1	159.8	10.1	26.6	7.9	151.0	5.8	7.0	18.914	15.627	38.843	169	2.5	10.5	60	18.544	15.581	38.415
39–40	7.2	168.8	9.8	36.0	8.5	128.3	6.2	8.0	18.895	15.631	38.811	139	2.7	15.2	66	18.403	15.575	38.286
44–45	7.0	157.8	10.5	23.9	8.2	132.9	5.5	6.7	18.921	15.630	38.835	161	2.5	8.4	56	18.490	15.463	38.191
49–50	7.3	144.1	7.6	35.8	8.4	119.9	5.9	8.2	18.890	15.631	38.800	128	2.9	14.1	63	18.435	15.581	38.300

[a]Leachate concentrations are reported relative to the initial bulk sediment mass.

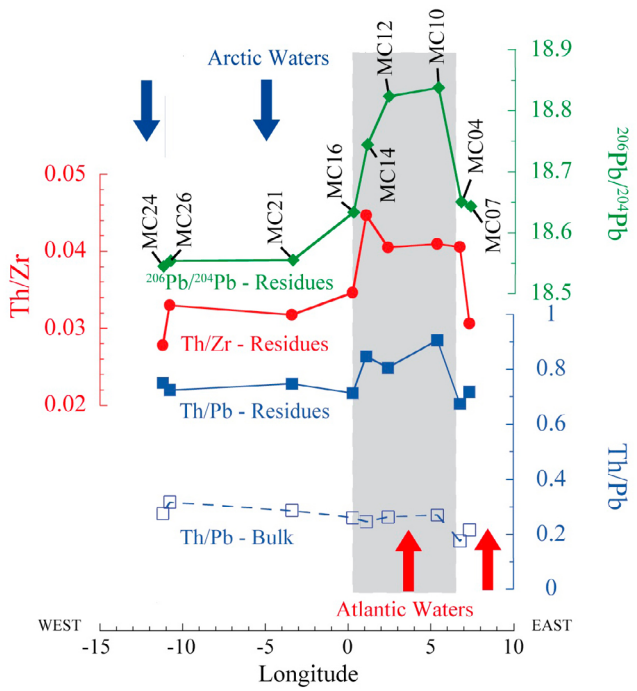

Figure 4. Th/Zr (red), Th/Pb (blue), and $^{206}Pb/^{204}Pb$ (green) ratios of surface sample detrital residues and Th/Pb ratios of bulk fractions. Sample sites follow the transect illustrated in Figure 1 and their geochemical and isotopic compositions display a spatial zonation in the Strait. Arrows illustrate the main active currents.

record, Pb isotope data from the residues display distinct trends, with a change in trend direction between sediments deposited before and after the start of the YD, at ~13 ka, located at about 20 cm. Below this depth (i.e., throughout the LGM early deglacial interval), $^{206}Pb/^{204}Pb$ ratios increased erratically with decreasing age, defining a "LGM/late glacial" trend (Trend A). In contrast, above the YD (i.e., since ~12 cal. ka), $^{206}Pb/^{204}Pb$ ratios decreased rather steadily, defining a "Holocene" trend (Trend B). These trends are clearly distinguished in the Pb isotope mixing diagram (Figure 6). Each reflects a dominantly binary mixing system with a common high $^{206}Pb/^{204}Pb$ end-member resulting in a total of three end-members. End-member 1, common to both trends, has isotopic compositions of $^{206}Pb/^{204}Pb \geq 18.8$ and $^{208}Pb/^{206}Pb \leq 2.06$ (Figure 7). End-member 2, from Trend A, displays $^{206}Pb/^{204}Pb \leq 18.4$ and $^{208}Pb/^{206}Pb \geq 2.085$. End-member 3, from Trend B, has $^{206}Pb/^{204}Pb \leq 18.6$ and $^{208}Pb/^{206}Pb \geq 2.085$.

[23] Three isotopic excursions are recorded in the residues from MC16. The sample at 20 cm (i.e., during the YD interval considering the age uncertainty, Figure 2) displays higher $^{206}Pb/^{204}Pb$ ratios whereas samples at 28 and 36 cm (~16.4 and ~19.8 cal. ka, respectively), exhibit lower $^{206}Pb/^{204}Pb$ ratios (Figure 5). Particular Pb isotopic compositions were also observed for samples from levels 23 and 38 cm (~14.3 and ~20.7 cal. ka, respectively) which plot along Trend B (Figure 6) whereas the other samples below the YD layer plot along Trend A. This suggests a switch of the source regions to end-members 1 and 3 during the deposition of these two samples. Finally, we note that two extreme excursions, at 25 and 38 cm, were also observed in one of the three analyzed subsamples at each of these levels (Table 4). However, these subsamples also displayed unusually high Pb concentrations and the other subsamples failed to reproduce the anomalous results. Thus while we cannot completely exclude the possibility of extreme sample heterogeneity, we believe that the most likely explanation of these surprising results is sample contamination and therefore they are not plotted in the figures and we will not discuss them further.

[24] Below the YD layer, $^{206}Pb/^{204}Pb$ ratios in leachates are similar to those of the corresponding residues (Figure 5), and both leachates and residues plot along the same mixing trend (Trend A) in Figure 6. In contrast, above the YD layer, $^{206}Pb/^{204}Pb$ ratios in leachates tend to be lower than those of the corresponding residues. Surprisingly, the leachates from this section of the core also plot along Trend A in Figure 6, whereas the residues plot along Trend B.

4. Discussion

[25] In sections 4.1 and 4.2 we compare Pb isotopic compositions of Fram Strait sediments to those of basalts, marginal crustal rocks and other marine sequences (both bulk and residues). Considering that residues represent the detrital fraction, their compositions should be comparable to those of the eroding continental crust in their source regions. The Arctic Ocean is a semienclosed basin and major potential Arctic sources include Greenland, the Arctic Archipelago (Queen Elizabeth Islands), the Mackenzie region, the Chukchi Sea, the East Siberian Sea, the Laptev

Table 6. Elemental and Pb Isotopic Data From Total, Detrital, and Leachable Fractions from Surface Samples[a]

	Total				Residues							Leachates						
Sample Name	Al_{tot} (%)	Zr_{tot} ($\mu g/g$)	Th_{tot} ($\mu g/g$)	Pb_{tot} ($\mu g/g$)	Al (%)	Zr ($\mu g/g$)	Th ($\mu g/g$)	Pb ($\mu g/g$)	$^{206}Pb/^{204}Pb$	$^{207}Pb/^{204}Pb$	$^{208}Pb/^{204}Pb$	Al ($\mu g/g$)	Th ($\mu g/g$)	Pb ($\mu g/g$)	Removed Pb (%)	$^{206}Pb/^{204}Pb$	$^{207}Pb/^{204}Pb$	$^{208}Pb/^{204}Pb$
BC07	6.1	129.0	6.4	29.5	6.7	156.4	4.8	6.7	18.643	15.603	38.547	14	1.9	24.0	78	18.430	15.610	38.325
MC04	6.1	144.1	7.6	43.1	6.8	100.6	4.1	6.0	18.650	15.583	38.554	10	1.4	24.1	80	18.262	15.576	38.128
BC10	6.9	164.1	8.1	29.8	7.9	164.5	6.7	7.4	18.837	15.617	38.800	113	2.0	24.4	77	18.391	15.619	38.347
BC12	7.2	134.6	8.1	30.7	8.4	154.3	6.2	7.8	18.823	15.613	38.817	16	2.4	21.1	73	18.481	15.603	38.417
BC14	7.2	139.7	8.1	33.1	8.3	133.5	6.0	7.0	18.744	15.602	38.739	15	2.6	26.7	79	18.457	15.612	38.399
MC16	7.0	137.9	7.3	28.0	7.9	152.5	5.3	7.4	18.633	15.601	38.628	12	2.3	25.2	77	18.472	15.608	38.403
MC21	6.7	177.6	7.1	24.8	7.5	164.5	5.2	7.0	18.556	15.582	38.553	12	2.5	18.4	72	18.466	15.599	38.427
MC24	6.7	171.4	7.8	24.6	7.6	161.2	5.3	7.4	18.553	15.581	8.657	12	2.4	18.3	71	18.457	15.606	38.420
MC26	6.5	191.7	7.0	25.4	7.4	190.3	5.3	7.0	18.545	15.581	38.580	12	2.0	17.6	71	18.407	15.602	38.369

[a]Leachate concentrations are reported relative to the initial bulk sediment mass.

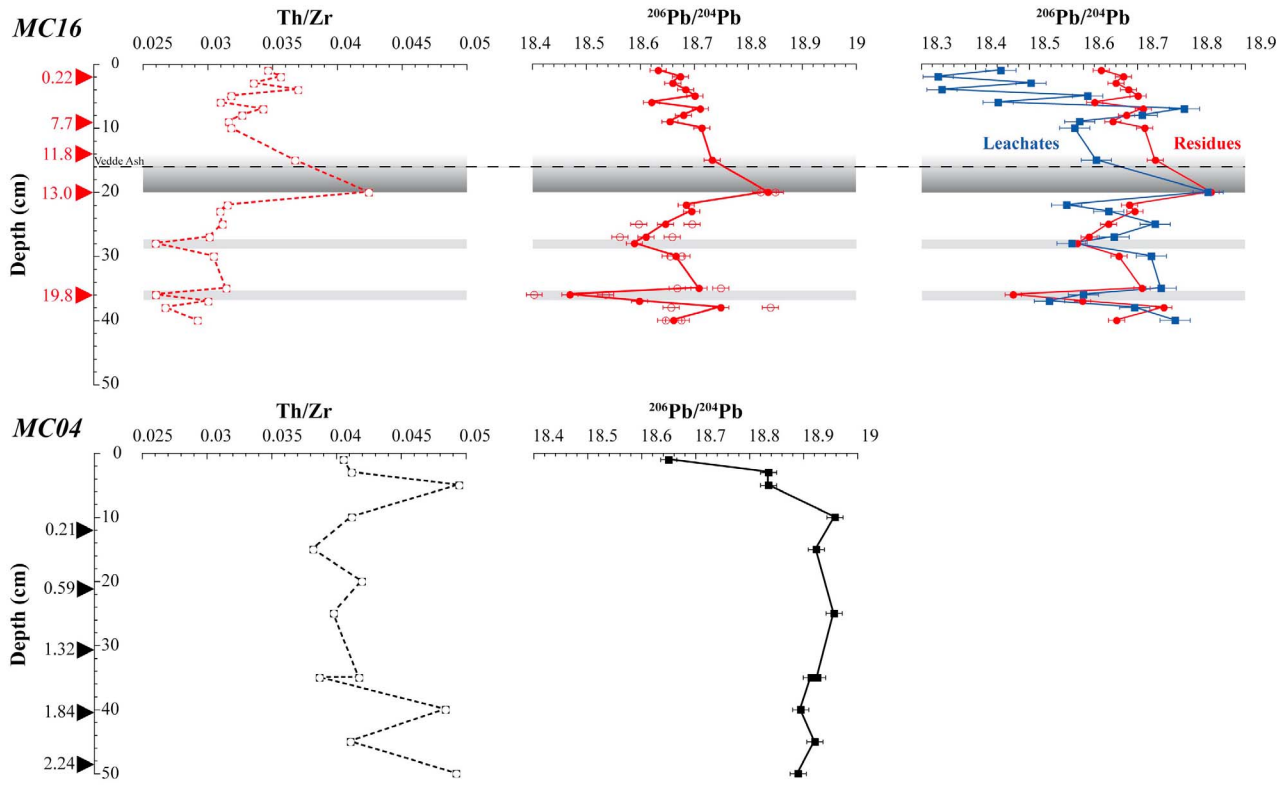

Figure 5. Th/Zr and $^{206}Pb/^{204}Pb$ profiles of cores MC04 and MC16 against depth. Red and black arrows represent calibrated ages (ka) in cores MC16 and MC04, respectively. Note the difference in sedimentation rate between the two cores. Graded gray bar represents the Younger Dryas event and thin light gray bars represent the 16.4 ka (28 cm) and 19.8 ka (36 cm) excursions. (left) Th/Zr ratios in cores (top) MC16 (open red squares) and (bottom) MC04 (open black squares). (middle) $^{206}Pb/^{204}Pb$ ratios in residues from cores (top) MC16 (red circles) and (bottom) MC04 (black squares). Open red circles represent replicate analyses of residues from core MC16 and solid circles represent the mean value. (right) $^{206}Pb/^{204}Pb$ ratios in residues (red circles) and leachates (blue squares) from core MC16. Blue open squares represent leachate replicates. Solid symbols represent the mean values of both residues and leachates.

Sea, the Kara Sea, the Barents Sea and Svalbard. Atlantic sources include Scandinavia, northwestern Europe and the Barents Sea (Figure 1). Unfortunately, only limited Pb isotopic data are available for many of these areas. Nevertheless, these data provide important constraints on the provenance of material delivered to Fram Strait though IRD.

4.1. The Sedimentary Domains

[26] Pb isotope compositions coupled with selected geochemical ratios allow distinction between Atlantic and Arctic sedimentary inputs that are controlled by the main active currents in the Strait (Figure 4). The bidirectional flow through Fram Strait leads to a zonation in the sedimentary supply as a function of longitude within the Strait. Geochemical and Pb isotopic compositions of surface sediments define the sedimentary domains under the present-day current pathways. Pb isotopes of surface samples from cores MC07 and MC04, located on the continental slope off the Spitsbergen margin (Figure 1 inset), plot along a linear trend defined by Pb isotope compositions of the Svalbard basalts and the Pan-African crust of northwestern Europe [*Fagel et al.*, 2004] (Figure 7a) suggesting that the North Atlantic Current (NAC) and the WSC control sedimentary fluxes in this area. Further to the west, under the influence of incoming waters from the GIN seas, distinctly higher $^{206}Pb/^{204}Pb$ ratios are observed in surface samples from cores MC10, 12 and 14 (Figure 4 and Table 6). They point to a stronger contribution from the western European Pan-African crust (Figure 7a). The central and western parts of Fram Strait are unquestionably influenced by both surface and deep currents from the Arctic Ocean [*Darby and Zimmerman*, 2008; *Darby et al.*, 2002; *Rudels et al.*, 2000]. This is evident in the fact that sediments from cores MC21, 24 and 26 have higher $^{208}Pb/^{206}Pb$ and lower $^{206}Pb/^{204}Pb$ than those from cores further to the east (Figure 4), possibly reflecting a contribution from the Pan-African Greenland crust (Figure 7a).

[27] The surface sample from core MC16 displays a Pb isotopic composition very similar to those in cores MC04 and MC07 (Figure 4). However, regarding the difference in sedimentation rates, the first cm of core MC16 would correspond to the top 10 cm of core C04 which, except for the surface, are distinct from core MC16. Cores MC04 and MC16 belong to distinct sedimentary domains and must be fed by different sedimentary source regions.

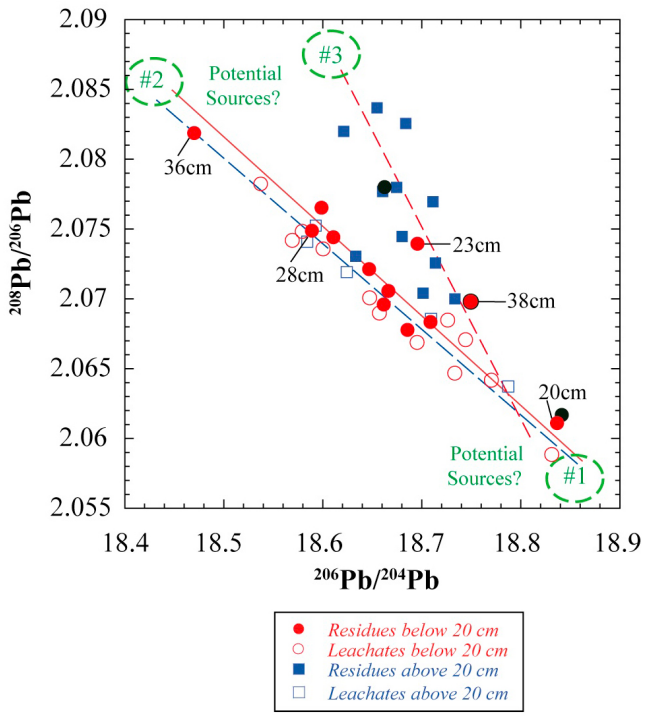

Figure 6. $^{208}Pb/^{206}Pb$ versus $^{206}Pb/^{204}Pb$ of leachates (open symbols) and residues (solid symbols) from core MC16. Due to the strong anthropogenic contribution, leachate samples from the mixed layer are not represented. Red circles represent leachates and residues of samples below 20 cm, the onset of the Younger Dryas. Blue squares represent leachates and residues of samples above 20 cm. Fields for the three main potential sources are identified in green dashed circles. Indicated samples correspond to the isotopic excursions discussed in the text (numbers refer to depths). Black circles represent the replicate values from the sample at 38 cm and highlight the heterogeneity of this sample although both analyses plot on the same trend. The red circle outlined in black represents the average of these two analyses.

4.2. Temporal Variations

[28] Core MC04 is located on the continental slope off Svalbard and presents a sedimentation rate ~15 times higher than that of core MC16. In addition, the sea ice cover over core MC04 is much less extensive than that over core MC16 [*Müller et al.*, 2009]. All of these considerations suggest that sediment transport mechanisms should be different between core MC16 and core MC04. Therefore MC16 sedimentation is thought to be mainly derived from Arctic sea ice. Pb isotopes from core MC04 display few variations suggesting constant supplies over the last two millennia. $^{206}Pb/^{204}Pb$ ratios suggest that core MC04 was mostly influenced by sediments derived from the Pan-African crust of western Europe through northward flowing currents. Since core MC16 provides a record since the LGM and because it reflects Arctic and/or proximal Greenland inputs and their variations since the LGM, we will focus the discussion on data from core MC16, in central Fram Strait.

4.2.1. Detrital Residues: Identification of Potential Source Regions

[29] The Pb isotopic compositions of the detrital residues from core MC16 are not randomly distributed within the mixing field delimited by the three end-members defined above. Instead they define two distinct trends, prior to and after the YD interval, with each trend representing a mixture of only two of the end-members. This rather abrupt change in the mixing pattern suggests a major change in sediment sources and thus in ice-drifting pathways.

[30] The three end-members have been tentatively assigned to specific circum-Arctic sources based on (limited) data available in the literature. As illustrated in Figure 7b, total and silicate fractions of surface sediments from Alpha-Ridge, in the Canadian basin north of Ellesmere Island, have Pb isotope ratios close to those of end-member #1 [*Winter et al.*, 1997]. Alpha-Ridge sediments are thought to be derived from the Queen Elizabeth Islands. River sediments from the Mackenzie and the Red Arctic rivers [*Millot et al.*, 2004] and marine sediments from the Canadian Basin (*Gartside* [1996], *Gobeil et al.* [2001], (Stations 11 and 18), and *Gueibe* [2009]) display $^{206}Pb/^{204}Pb$ and $^{208}Pb/^{206}Pb$ ratios that plot on or near Trend A . Samples from the Arctic Mendeleyev (Station 26) and Lomonosov (Station 35) Ridges [*Gobeil et al.*, 2001] plot slightly off Trend A but not far from end-member 1, providing further evidence that this end-member indeed corresponds to Canadian Arctic sources.

[31] River sediments from the Lena display Pb isotopic compositions consistent with end-member 2 (Figure 7b). The Pb isotopic compositions of basalts from the Norilsk region [*Lightfoot et al.*, 1993; *Wooden et al.*, 1993] and of samples from the Siberia region [*Winter et al.*, 1997, and references therein] both define large fields in the top left corners of Figures 7a and 7b that could encompass end-member 2. The Kathanga River, which drains the Norilsk region, as well as the above mentioned Lena river, end in the Laptev sea. We thus assign end-member 2 to the Central Siberia/Laptev Sea source area.

[32] The Greenland Pan-African crust appears to be the most likely source matching end-member 3 (Figure 7b). Trend B, which is essentially a mixture between end-members 1 and 3, shows higher variability (R^2 of 0.64 for the linear regression) than Trend A (R^2 of 0.85). Some contributions from end-member 2 might explain this higher variability.

[33] Results from previous studies tend to corroborate our source identification. *Darby et al.* [2002] and *Darby and Zimmerman* [2008] identified Fe-oxide grains and sediments from IRD events in a core very close to MC16 (core PS1230, Figure 1), which they linked to a Northern Canada and Queen Elizabeth Islands provenance. These authors also provide evidence for sediment inputs from the Siberian margin (e.g., Laptev Sea) region. Thus their results are coherent with the end-members 1 and 2 that we have defined based on Pb isotope compositions.

4.2.2. Isotopic Excursions

[34] Considering the estimated sedimentation rate of core MC16, from 1.1 to 5 cm/ka, each sample represents a time period of a few hundred years, assuming that mixing by bioturbation remained negligible until recent time, when productivity increased drastically [*Zamelczyk et al.*, 2010]. Thus changes in isotopic compositions at the level of the 1 cm sampling slices are considered to illustrate paleogeographical

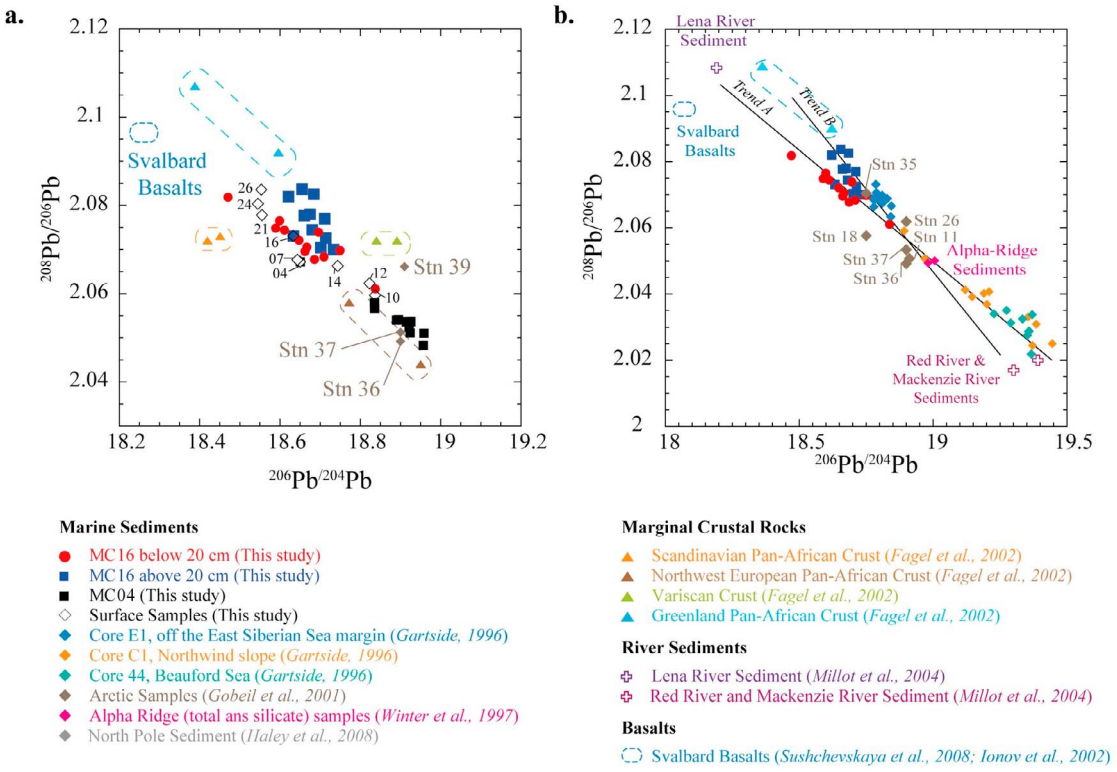

Figure 7. $^{208}Pb/^{206}Pb$ versus $^{206}Pb/^{204}Pb$ diagram illustrating the detrital trends along with data from the literature for marine sediments and potential source regions. (a) GIN Seas and European sources along with residues from cores MC04 and MC16 and surface sediments. (b) Arctic sources and sediments along with residues from core MC16.

events of a few hundred years duration. Pb isotope ratios measured at 28 cm and 36 cm downcore tend toward end-member 2, thus suggesting enhanced contributions from the Laptev/Siberian source area at ca 16.4 and 19.8 ka, respectively. In contrast, the isotopic composition at 20 cm tends toward end-member 1 suggesting strong contributions from the Canadian Arctic region during the interval assigned to the YD. Unlike the other pre-YD samples, sediment residues at 23 and 38 cm (at ca 14.3 and 20.7 ka respectively) plot along Trend B (Figure 6). This might suggest a pulse from end-member 3, that is, from Greenland, possibly linked to the LGM extreme Greenland Ice advance, or more simply it might correspond to an isolated calved iceberg. However, we remain cautious regarding this interpretation since duplicate analyses of the sample at 38 cm produced distinct values that do not agree within analytical uncertainty. Enhanced heterogeneity of the sediment at this level, possibly linked to a large but rapid paleoceanographic event at ~20.7 ka, might explain this lack of reproducibility. *Darby et al.* [2002] and *Darby and Zimmerman* [2008] report evidence for a glacial event at about that time. We note that the two results obtained from the sample at 38 cm, though disagreeing beyond analytical uncertainty, both plot along Trend B, which would be consistent with a Greenland contribution.

[35] *Darby and Zimmerman* [2008] also note some features suggestive of contributions from Laptev/Siberian sources in the sediments from 16.4 and 19.8 ka, which would be consistent with the Laptev/Siberian geochemical component that we see in these excursions (Figure 6, samples at 28 and 36 cm). According to recent paleogeographical reconstructions [*Hubberten et al.*, 2004; *Siegert and Marsiat*, 2001; *Siegert et al.*, 1999; *Spielhagen et al.*, 2004], the extent of the ice sheet over northern Siberia was limited to the Barents Sea and the eastern part of the Kara Sea during this time interval. Cold and dry conditions would have prevailed over the emerged Laptev Sea. Therefore, transport of material from the Laptev Sea through ice rafting does not seem to be a viable explanation for these isotopic excursions. On the other hand, a freshwater event in the Kara Sea and the Arctic Ocean at ~15.8 ka has been recently reported, resulting from the drainage of the Chuya Katun lake through the Ob river, into the Kara sea [*Reuther et al.*, 2006]. Since we cannot distinguish between the Kara and Laptev Sea source signatures, this event cannot be ruled out as a possible contributor to the 16.4 ka excursion, given the age uncertainties.

4.2.3. Leachates

[36] In the mixed layer, the anthropogenic Pb signal overprints the natural signal as illustrated by the higher Pb content of sediments and lower $^{206}Pb/^{204}Pb$ of leachates in this interval. In the following discussion, data from the mixed layer will hence be excluded and only preanthropogenic data will be discussed.

[37] Another issue that must be examined is the possibility that the leaching procedure leads to some contamination of leachates by Pb derived from the detrital fraction, in which case the leachates would not represent the purely authigenic component. Two distinct approaches can be used to address this issue. The first, the Al/Ti test, suggested by *Bayon et al.*

[2002] to estimate detrital contributions to leachates, is uninformative here, because Ti concentrations in leachates are often below detection limits. Nonetheless, such very low Ti contents (<0.001%) already suggest that detrital contributions to leachates must be small. An alternative approach involves mass balance calculations following the procedure of *Gutjahr et al.* [2007], using Sr isotopic compositions in both the detrital and leached fractions, and assuming that the Sr isotopic composition of the leachate should be that of seawater. Based on our Sr isotope data (that will be published elsewhere) we demonstrate that the detrital phase may contribute an average of 20% of the leachate Sr. Based on the hypothesis that Pb would behave as Sr does, this level of contamination would modify $^{206}Pb/^{204}Pb$ values in leachates by up to 0.025. We thus decided to include this uncertainty in the calculation of error bars of leachate Pb isotope ratios. Values reported for leachates can therefore be considered to represent Pb inherited through exchange with seawater (henceforth referred to as "authigenic" Pb in contrast with the "detrital" Pb), within the shown uncertainty (Figure 5).

[38] Pb isotopic compositions in the authigenic versus detrital fractions varied differently through time. In the pre-YD section of MC16, they track each other quite well (Figure 5). In contrast, in the post-YD interval, they diverge increasingly toward core top. Whereas Pb isotopes in detrital fractions follow two distinct trends with one common end-member, as discussed above, those from the authigenic fraction define a single binary mixing system (Figure 6, R^2 of 0.97), broadly coincident with Trend A from the residue data. Potential sources of the authigenic Pb in leachates are thus likely to be the same as those of end-members 1 and 2 defined for the residues ($^{206}Pb/^{204}Pb \geq 18.9$ and $^{208}Pb/^{206}Pb \leq 2.06$, and $^{206}Pb/^{204}Pb \leq 18.3$ and $^{208}Pb/^{206}Pb \geq 2.09$, respectively). The similarity between the Pb isotope values of leachate end-members and detrital end-members 1 and 2 suggests that the water masses developed their Pb isotope signature through exchange with particulate and dissolved fluxes from the Canadian/Mackenzie area and/or the Siberian/Lena area. As discussed above, dissolution of Fe-Mn oxyhydroxide precipitates should account for most of the Pb recovered during the second step of the leaching procedure. Such precipitates may partly form in the water column but are mostly generated by early diagenetic effects at the water-sediment interface [*Bayon et al.*, 2002; *Gutjahr et al.*, 2007].

[39] It is perhaps surprising that leachates do not exhibit a more radiogenic Pb signature than the residues, in contrast to what has been observed in the Northwest Atlantic region [*Gutjahr et al.*, 2009; *Gutjahr et al.*, 2008; *Kurzweil et al.*, 2010; *von Blanckenburg and Nägler*, 2001]. The pre-YD samples show no coherent pattern as leachates can be either more or less radiogenic than the corresponding residues, while the post-YD leachates are clearly less radiogenic than their residues. In the Arctic Ocean, *Haley et al.* [2008] suggested that the less radiogenic Pb signal found in leachates reflects glacial remobilization of erosional products of the Siberian basalts. Subsequent partial exchange with these particles would have imprinted the water masses in a way similar to that which is thought to occur for Nd [*Lacan and Jeandel*, 2004a, 2004b]. Indeed, though Pb and Nd are not completely analogous as illustrated by their different marine residence times, Nd isotopic exchange between dissolved and particulate phases along continental margins might shed some light on Pb isotope behavior (see for example *Arsouze et al.* [2009], *Lacan and Jeandel* [2005], and *Tachikawa et al.* [1999]). The results of these studies suggest that the isotopic compositions of highly particle-reactive elements such as Th, Pa, Pb and Nd, along continental margins, could be controlled by adsorption/desorption processes through water/particle exchange. Perhaps such exchange processes partially explain the lack of a systematic difference between the Pb isotopic compositions of leachates and residues. The leachate data would hence reflect the ambient water mass signature, however this signature would be acquired by exchange with particles at sites with high particle flux such as continental margins.

[40] Data from MC16 (preanthropogenic) leachates could suggest that Pb isotopic signatures carried by deep-water masses were acquired through such "boundary exchange" processes off the Siberian margin and/or off the Canadian/Mackenzie margin area, i.e., at sites where major particulate fluxes from either paleo ice margins or large river systems occurred. We suggest that the Pb fractions from MC16 core leachates were inherited from the ambiant water masses circulating over the sediment, i.e., the Arctic deep-water. Leachate data define a single mixing line suggesting that, unlike for the residues, the two sources thought to imprint the leachate signature have not changed since the LGM period. Nevertheless, changes did occur in the relative contribution of each end-member.

[41] In conclusion, we think that the Pb isotopic composition of the leachates (i.e., exchangeable fraction) precipitates from ambient seawater, hence recording the properties of dissolved metals in the sediment carrier water mass. However, the water mass itself is thought to acquire this geochemical signature through adsorption/dissolution processes with particles during its trajectory through circum-Arctic sites where high particulate fluxes occur (off major rivers today).

4.3. Paleoceanographic Implications

[42] The two trends defining the three sources of particulate material exported through Fram Strait are interpreted in relation to ice-rafting deposition and thus sea ice and/or iceberg routes. The pre-YD interval sediments originated from the Canadian/Mackenzie (end-member 1) and Siberian (end-member 2) margins. Maximum influence of the Siberian margins occurred during the isotopic excursions at ca. 16.4 and 19.8 ka. During the post-YD interval (Trend B), particulate supplies seem to have been mostly derived from Canadian/Mackenzie (end-member 1) and Greenland (end-member 3) sources. The YD itself was apparently an interval with maximum and prominent input from the Canadian/Mackenzie source area (end-member 1).

[43] Recent studies have proposed a northward meltwater pulse from the Laurentide Ice Sheet through the Mackenzie river system during the YD [*Murton et al.*, 2010; *Teller et al.*, 2005]. It has also been suggested that this pulse destabilized the ice pack and enhanced sea ice flux through the Beaufort Gyre. (Not and Hillaire-Marcel, submitted manuscript, 2011). Two consequences resulting from such a pulse are worth noting: 1) an increased flux of sedimentary material along the ice-rafting route notably over the central Lomonosov Ridge [*Hanslik et al.*, 2010; Not and Hillaire-

Marcel, submitted manuscript, 2011] and western Fram Strait (site MC16), and 2) a probable increased freshwater/sea ice export through Fram Strait toward the GIN Seas likely to drastically reduce the AMOC [*Tarasov and Peltier*, 2005, 2006].

[44] In fact, studies of the Northwind Ridge sediment, off the Chukchi Sea [*Polyak et al.*, 2007; *Polyak et al.*, 2009], have also suggested the presence of 1) a gyre type circulation over the western basin of the Arctic Ocean during the LGM/early deglacial period coexisting with 2) a Trans-Polar Drift type circulation from the Eurasian basin [*Polyak et al.*, 2009; *Spielhagen et al.*, 2004]. This would produce a sea ice circulation pattern in agreement with our Trend A described above. The short Pb isotopic excursions during this interval might relate to events such as ice surging and/or drainage events from the Siberian margin area [*Darby et al.*, 2002].

[45] Several events, along with the YD, occurred during the LGM/deglacial intervals and have likely contributed to changes in sea ice and iceberg routes of the Arctic: 1) the final deglaciation of the Svalbard-Barents Sea Ice Sheet which presumably occurred at ~13–15 ka [*Elverhøi et al.*, 1998; *Hubberten et al.*, 2004], 2) the opening of Bering Strait at ~13.5 ka [*England and Furze*, 2008], and 3) the sea level rise subsequent to meltwater pulse 1a at ~14.5 ka. Because of the sea level rise and of the new circulation dynamic after the YD, most of the Siberian margins were at least partially submerged notably the Barents Sea area where sea ice could have been directly exported from the Arctic Ocean, depending on the atmospheric regime [*Hilmer et al.*, 1998].

[46] During the post-YD interval, increasing relative particulate supplies probably from Greenland (versus Canadian sources) are observed at the MC16 site (Trend B). As recently documented by *Larsen et al.* [2010] and *Möller et al.* [2010], the Holocene seems to have been characterized by an eastward drift from northern Greenland toward Fram Strait. This may have been responsible for the enhanced supply of detritus from the Greenland margin and the concomitant relative decrease of the Siberian source material.

[47] Deep water circulation patterns, as illustrated by exchangeable Pb isotopes from leachates (Figure 6), seem to have been much less variable through time. This is illustrated by the fact that the data fit a single mixing line, indicating that deep water masses were influenced by particulate fluxes from both the Canadian margin (end-member 1) and the Siberian margin (end-member 2). However, the relative contributions of the two end-members fluctuated substantially (Figure 5, top right). This supports the above interpretation that the Pb isotopic signatures of the deep water masses were acquired by exchange processes in regions with high particulate fluxes.

5. Conclusions

[48] This study has demonstrated the ability of geochemical tracers and Pb isotopes in deep-sea sediments to provide insights into paleoceanographical events that occurred during the deglaciation of the circum Arctic, and the Holocene. Indeed, leachable fractions (at core depths below anthropogenic influence) have isotopic signatures acquired by deep water masses near the continental margins of the Arctic Ocean, whereas residual detrital fractions display isotopic compositions inherited from sediment source areas and thus document sedimentary fluxes toward and across the Arctic Ocean.

[49] This detrital fraction, mainly transported by ice, illustrates relative contributions from three end-members (Canada, Siberia, and Greenland margins) that varied significantly through time, both gradually and during short events linked to specific ice margin instabilities. Our data argue for increasing influence of Greenland sediment supplies through the Holocene suggesting deflection of the Trans-Polar Drift westward toward the northern Greenland ice margin (with a weaker Beaufort gyre). The detrital fraction also records a strong isotopic excursion during the YD-interval, pointing to a trigger event in the Canada/Mackenzie area that resulted in enhanced Beaufort Gyre circulation, as is also recorded in sediments from the Lomonosov Ridge. (Not and Hillaire-Marcel, submitted manuscript, 2011). This supports the hypothesis of *Tarasov and Peltier* [2005, 2006] that an Arctic freshwater/sea ice pulse might have been at the origin of the AMOC collapse of this interval. We suggest that earlier isotopic excursions found in this core from the LGM to the YD-interval are mostly related to paleogeographical events along the Siberian margins. The low sedimentation rate of the studied core nevertheless limits more detailed paleoceanographic reconstructions.

[50] Ongoing complementary radiogenic isotope measurements (Nd, Sr) will provide tighter constraints on sediment sources and on how their relative importance varied through time.

[51] **Acknowledgments.** The present study is a contribution to the WarmPast and Past4Future projects. Funding by the Ministère du Développement Economique, de l'Innovation et de l'Exportation of Québec, and the Fonds Québécois de Recherche sur la Nature et les Technologies has been instrumental. J.M. also acknowledges support from the French Ministère de l'Education and the GEOTOP research network through Ph.D. awards. Complementary funding by NSERC-Canada (Discovery Grant CHM) is also acknowledged. Special thanks are due to Katrin Husum and Morten Hald (University of Tromsø) for their invitation to the 2006–2008 cruises of the Jan Mayen in the Fram Strait Area. Discussions with Katrin Husum and Katarzyna Zamelczyk (both from the University of Tromsø) and with Anne de Vernal (GEOTOP-UQAM) have been very helpful. We are grateful to Marcus Gutjahr, Julian Murton, and Natalie Fagel for their constructive suggestions that significantly improved the quality of this manuscript.

References

Arsouze, T., J. C. Dutay, F. Lacan, and C. Jeandel (2009), Reconstructing the Nd oceanic cycle using a coupled dynamical: Biogeochemical model, *Biogeosciences*, *6*(12), 2829–2846, doi:10.5194/bg-6-2829-2009.

Bayon, G., C. R. German, R. M. Boella, J. A. Milton, R. N. Taylor, and R. W. Nesbitt (2002), An improved method for extracting marine sediment fractions and its application to Sr and Nd isotopic analysis, *Chem. Geol.*, *187*(3–4), 179–199, doi:10.1016/S0009-2541(01)00416-8.

Birgel, D., and H. C. Hass (2004), Oceanic and atmospheric variations during the last deglaciation in the Fram Strait (Arctic Ocean): A coupled high-resolution organic-geochemical and sedimentological study, *Quat. Sci. Rev.*, *23*(1–2), 29–47, doi:10.1016/j.quascirev.2003.10.001.

Bonnet, S., A. de Vernal, C. Hillaire-Marcel, T. Radi, and K. Husum (2010), Variability of sea-surface temperature and sea ice cover in the Fram Strait over the last two millennia, *Mar. Micropaleontol.*, *74*(3–4), 59–74, doi:10.1016/j.marmicro.2009.12.001.

Broecker, W. S. (1991), The great ocean conveyor, *Oceanography (Wash. D.C.)*, *4*, 79–89.

Broecker, W. S., and T. H. Peng (1992), *Tracers in the Sea*, Lamont-Doherty Geol. Obs, Palisades, N. Y.

Carignan, J., C. Hillaire-Marcel, and A. De Vernal (2008), Arctic vs. North Atlantic water mass exchanges in Fram Strait from Pb isotopes in sediments, *Can. J. Earth Sci.*, *45*(11), 1253–1263, doi:10.1139/E08-050.

Darby, D. A., and P. Zimmerman (2008), Ice-rafted detritus events in the Arctic during the last glacial interval, and the timing of the Innuitian and Laurentide ice sheet calving events, *Polar Res.*, *27*(2), 114–127, doi:10.1111/j.1751-8369.2008.00057.x.

Darby, D. A., J. F. Bischof, R. F. Spielhagen, S. A. Marshall, and S. W. Herman (2002), Arctic ice export events and their potential impact on global climate during the late Pleistocene, *Paleoceanography*, *17*(2), 1025, doi:10.1029/2001PA000639.

Darby, D. A., L. Polyak, and H. A. Bauch (2006), Past glacial and interglacial conditions in the Arctic Ocean and marginal seas: A review, *Prog. Oceanogr.*, *71*(2–4), 129–144, doi:10.1016/j.pocean.2006.09.009.

Dickson, R., B. Rudels, S. Dye, M. Karcher, J. Meincke, and I. Yashayaev (2007), Current estimates of freshwater flux through Arctic and subarctic seas, *Prog. Oceanogr.*, *73*(3–4), 210–230, doi:10.1016/j.pocean.2006.12.003.

Dokken, T. M., and M. Hald (1996), Rapid climatic shifts during isotope stages 2–4 in the Polar North Atlantic, *Geology*, *24*(7), 599–602, doi:10.1130/0091-7613(1996)024<0599:RCSDIS>2.3.CO;2.

Elverhøi, A., J. A. Dowdeswell, S. Funder, J. Mangerud, and R. Stein (1998), Glacial and oceanic history of the polar north atlantic margins: An overview, *Quat. Sci. Rev.*, *17*(1–3), 1–10, doi:10.1016/S0277-3791(97)00073-5.

England, J. H., and M. F. A. Furze (2008), New evidence from the western Canadian Arctic Archipelago for the resubmergence of Bering Strait, *Quat. Res.*, *70*(1), 60–67, doi:10.1016/j.yqres.2008.03.001.

Fagel, N., C. Innocent, C. Gariepy, and C. Hillaire-Marcel (2002), Sources of Labrador Sea sediments since the last glacial maximum inferred from Nd-Pb isotopes, *Geochim. Cosmochim. Acta*, *66*(14), 2569–2581, doi:10.1016/S0016-7037(02)00866-9.

Fagel, N., C. Hillaire-Marcel, M. Humblet, R. Brasseur, D. Weis, and R. Stevenson (2004), Nd and Pb isotope signatures of the clay-size fraction of Labrador Sea sediments during the Holocene: Implications for the inception of the modern deep circulation pattern, *Paleoceanography*, *19*(3), PA3002, doi:10.1029/2003PA000993.

Fahrbach, E., J. Meincke, S. Østerhus, G. Rohardt, U. Schauer, V. Tverberg, and J. Verduin (2001), Direct measurements of volume transports through Fram Strait, *Polar Res.*, *20*(2), 217–224, doi:10.1111/j.1751-8369.2001.tb00059.x.

Flynn, W. W. (1968), The determination of low levels of polonium-210 in environmental materials, *Anal. Chim. Acta*, *43*(C), 221–227, doi:10.1016/S0003-2670(00)89210-7.

Foster, G. L., and D. Vance (2006), Negligible glacial-interglacial variation in continental chemical weathering rates, *Nature*, *444*(7121), 918–921, doi:10.1038/nature05365.

Fütterer, D. K. (2000), The solid phase of marine sediments, in *Marine Geochemistry*, edited by H. D. Schulz and M. Zabel, pp. 1–25, Springer, New York.

Gartside, M. (1996), Sources et inventaire du plomb anthropique dans les sédiments de l'Océan Arctique profond, M. S. Thesis, 79 pp., Univ. Québec à Montréal, Montréal, QB, Canada.

Ghaleb, B. (2009), Overview of the methods for the measurement and interpretation of short-lived radioisotopes and their limits, *IOP Conf. Ser. Earth Environ. Sci.*, *5*, 012007, doi:10.1088/1755-1307/1085/1081/012007.

Gobeil, C., R. W. Macdonald, J. N. Smith, and L. Beaudin (2001), Atlantic water flow pathways revealed by lead contamination in Arctic basin sediments, *Science*, *293*(5533), 1301–1304, doi:10.1126/science.1062167.

Gueibe, J. (2009), *Analyse minéralogiques et isotopiques (Nd, Pb) des sédiments de l'Océan Arctique (Ride de Mendeleev, carottes HOTRAX) en vue d'identifier les agents de transport océanique*, 95 pp., Univ. Libre de Bruxelles, Bruxelles.

Gutjahr, M., M. Frank, C. H. Stirling, V. Klemm, T. van de Flierdt, and A. N. Halliday (2007), Reliable extraction of a deepwater trace metal isotope signal from Fe-Mn oxyhydroxide coatings of marine sediments, *Chem. Geol.*, *242*(3–4), 351–370, doi:10.1016/j.chemgeo.2007.03.021.

Gutjahr, M., M. Frank, C. H. Stirling, L. D. Keigwin, and A. N. Halliday (2008), Tracing the Nd isotope evolution of North Atlantic Deep and Intermediate Waters in the western North Atlantic since the Last Glacial Maximum from Blake Ridge sediments, *Earth Planet. Sci. Lett.*, *266*(1–2), 61–77, doi:10.1016/j.epsl.2007.10.037.

Gutjahr, M., M. Frank, A. N. Halliday, and L. D. Keigwin (2009), Retreat of the Laurentide ice sheet tracked by the isotopic composition of Pb in western North Atlantic seawater during termination 1, *Earth Planet. Sci. Lett.*, *286*(3–4), 546–555, doi:10.1016/j.epsl.2009.07.020.

Haley, B. A., M. Frank, R. F. Spielhagen, and J. Fietzke (2008), Radiogenic isotope record of Arctic Ocean circulation and weathering inputs of the past 15 million years, *Paleoceanography*, *23*(1), PA1S13, doi:10.1029/2007PA001486.

Hanslik, D., M. Jakobsson, J. Backman, S. Björck, E. Sellén, M. O'Regan, E. Fornaciari, and G. Skog (2010), Quaternary Arctic Ocean sea ice variations and radiocarbon reservoir age corrections, *Quat. Sci. Rev.*, *29*(25–26), 3430–3441, doi:10.1016/j.quascirev.2010.06.011.

Harlavan, Y., and Y. Erel (2002), The release of Pb and REE from granitoids by the dissolution of accessory phases, *Geochim. Cosmochim. Acta*, *66*(5), 837–848, doi:10.1016/S0016-7037(01)00806-7.

Harlavan, Y., Y. Erel, and J. D. Blum (1998), Systematic changes in lead isotopic composition with soil age in glacial granitic terrains, *Geochim. Cosmochim. Acta*, *62*(1), 33–46, doi:10.1016/S0016-7037(97)00328-1.

Hebbeln, D. (2000), Flux of ice-rafted detritus from sea ice in the Fram Strait, *Deep Sea Res., Part II*, *47*(9–11), 1773–1790, doi:10.1016/S0967-0645(00)00006-0.

Hebbeln, D., and H. Berner (1993), Surface sediment distribution in the Fram Strait, *Deep Sea Res., Part I*, *40*(9), 1731–1745, doi:10.1016/0967-0637(93)90029-3.

Hebbeln, D., and G. Wefer (1997), Late Quaternary paleoceanography in the Fram Strait, *Paleoceanography*, *12*(1), 65–78, doi:10.1029/96PA02753.

Hebbeln, D., T. Dokken, E. S. Andersen, M. Hald, and A. Elverhøi (1994), Moisture supply for northern ice-sheet growth during the last glacial maximum, *Nature*, *370*(6488), 357–360, doi:10.1038/370357a0.

Henderson, G. M., and E. Maier-Reimer (2002), Advection and removal of 210Pb and stable Pb isotopes in the oceans: A general circulation model study, *Geochim. Cosmochim. Acta*, *66*(2), 257–272, doi:10.1016/S0016-7037(01)00779-7.

Hilmer, M., M. Harder, and P. Lemke (1998), Sea ice transport: A highly variable link between Arctic and North Atlantic, *Geophys. Res. Lett.*, *25*(17), 3359–3362, doi:10.1029/98GL52360.

Hubberten, H. W., et al. (2004), The periglacial climate and environment in northern Eurasia during the Last Glaciation, *Quat. Sci. Rev.*, *23*(11–13), 1333–1357, doi:10.1016/j.quascirev.2003.12.012.

Husum, K. (2006), Marine geological cruise to West Spitsbergen Margin and Fram Strait: RV "Jan Mayen" 11–19 October 2006, *Cruise Rep. JM06-WP*, 40 pp., Univ. of Tromsø, Tromsø, Norway.

Jones, E. P. (2001), Circulation in the Arctic Ocean, *Polar Res.*, *20*(2), 139–146, doi:10.1111/j.1751-8369.2001.tb00049.x.

Jones, E. P., B. Rudels, and L. G. Anderson (1995), Deep waters of the Arctic Ocean: Origins and circulation, *Deep Sea Res., Part I*, *42*(5), 737–760, doi:10.1016/0967-0637(95)00013-V.

Kurzweil, F., M. Gutjahr, D. Vance, and L. Keigwin (2010), Authigenic Pb isotopes from the Laurentian Fan: Changes in chemical weathering and patterns of North American freshwater runoff during the last deglaciation, *Earth Planet. Sci. Lett.*, *299*(3–4), 458–465, doi:10.1016/j.epsl.2010.09.031.

Lacan, F., and C. Jeandel (2004a), Denmark Strait water circulation traced by heterogeneity in neodymium isotopic compositions, *Deep Sea Res., Part I*, *51*(1), 71–82, doi:10.1016/j.dsr.2003.09.006.

Lacan, F., and C. Jeandel (2004b), Neodymium isotopic composition and rare earth element concentrations in the deep and intermediate Nordic Seas: Constraints on the Iceland Scotland Overflow Water signature, *Geochem. Geophys. Geosyst.*, *5*(11), Q11006, doi:10.1029/2004GC000742.

Lacan, F., and C. Jeandel (2005), Neodymium isotopes as a new tool for quantifying exchange fluxes at the continent-ocean interface, *Earth Planet. Sci. Lett.*, *232*(3–4), 245–257, doi:10.1016/j.epsl.2005.01.004.

Larsen, N. K., K. H. Kjaer, S. Funder, P. Möller, J. J. M. van der Meer, A. Schomacker, H. Linge, and D. A. Darby (2010), Late Quaternary glaciation history of northernmost Greenland-Evidence of shelf-based ice, *Quat. Sci. Rev.*, *29*, 3399–3414, doi:10.1016/j.quascirev.2010.07.027.

Lightfoot, P. C., C. J. Hawkesworth, J. Hergt, A. J. Naldrett, N. S. Gorbachev, V. A. Fedorenko, and W. Doherty (1993), Remobilisation of the continental lithosphere by a mantle plume: Major-, trace-element, and Sr-, Nd-, and Pb-isotope evidence from picritic and tholeiitic lavas of the Noril'sk District, Siberian Trap, Russia, *Contrib. Mineral. Petrol.*, *114*(2), 171–188, doi:10.1007/BF00307754.

Manhes, G., C. J. Allègre, B. Dupré, and B. Hamelin (1980), Lead isotope study of basic-ultrabasic layered complexes: Speculations about the age of the earth and primitive mantle characteristics, *Earth Planet. Sci. Lett.*, *47*(3), 370–382, doi:10.1016/0012-821X(80)90024-2.

McManus, J. F., R. Francois, J. M. Gherardl, L. Kelgwin, and S. Drown-Leger (2004), Collapse and rapid resumption of Atlantic meridional circulation linked to deglacial climate changes, *Nature*, *428*(6985), 834–837, doi:10.1038/nature02494.

Millot, R., C. J. Allègre, J. Gaillardet, and S. Roy (2004), Lead isotopic systematics of major river sediments: A new estimate of the Pb isotopic composition of the Upper Continental Crust, *Chem. Geol.*, *203*(1–2), 75–90, doi:10.1016/j.chemgeo.2003.09.002.

Möller, P., N. K. Larsen, K. H. Kjær, S. Funder, A. Schomacker, H. Linge, and D. Fabel (2010), Early to middle Holocene valley glaciations on the

northernmost Greenland, *Quat. Sci. Rev.*, *29*, 3379–3398, doi:10.1016/j.quascirev.2010.06.044.

Müller, J., G. Massé, R. Stein, and S. T. Belt (2009), Variability of sea ice conditions in the Fram Strait over the past 30,000 years, *Nat. Geosci.*, *2*(11), 772–776, doi:10.1038/ngeo665.

Murton, J. B., M. D. Bateman, S. R. Dallimore, J. T. Teller, and Z. Yang (2010), Identification of Younger Dryas outburst flood path from Lake Agassiz to the Arctic Ocean, *Nature*, *464*(7289), 740–743, doi:10.1038/nature08954.

Peltier, W. R., G. Vettoretti, and M. Stastna (2006), Atlantic meridional overturning and climate response to Arctic Ocean freshening, *Geophys. Res. Lett.*, *33*(6), L06713, doi:10.1029/2005GL025251.

Polyak, L., D. A. Darby, J. F. Bischof, and M. Jakobsson (2007), Stratigraphic constraints on late Pleistocene glacial erosion and deglaciation of the Chukchi margin, Arctic Ocean, *Quat. Res.*, *67*(2), 234–245, doi:10.1016/j.yqres.2006.08.001.

Polyak, L., et al. (2009), Late Quaternary stratigraphy and sedimentation patterns in the western Arctic Ocean, *Global Planet. Change*, *68*(1–2), 5–17, doi:10.1016/j.gloplacha.2009.03.014.

Reimer, P. J., et al. (2009), IntCal09 and Marine09 radiocarbon age calibration curves, 0–50,000 years CAL BP, *Radiocarbon*, *51*(4), 1111–1150.

Reuther, A. U., J. Herget, S. Ivy-Ochs, P. Borodavko, P. W. Kubik, and K. Heine (2006), Constraining the timing of the most recent catalysmic flood event from ice-dammed lakes in the Russian Altai Mountains, Siberia, using cosmogenic in situ 10Be, *Geology*, *34*(11), 913–916, doi:10.1130/G22755A.1.

Rudels, B., R. Meyer, E. Fahrbach, V. V. Ivanov, S. Østerhus, D. Quadfasel, U. Schauer, V. Tverberg, and R. A. Woodgate (2000), Water mass distribution in Fram Strait and over the Yermak Plateau in summer 1997, *Ann. Geophys.*, *18*(6), 687–705, doi:10.1007/s00585-000-0687-5.

Rudels, B., E. P. Jones, U. Schauer, and P. Eriksson (2004), Atlantic sources of the Arctic Ocean surface and halocline waters, *Polar Res.*, *23*(2), 181–208, doi:10.1111/j.1751-8369.2004.tb00007.x.

Rudels, B., G. Björk, J. Nilsson, P. Winsor, I. Lake, and C. Nohr (2005), The interaction between waters from the Arctic Ocean and the Nordic Seas north of Fram Strait and along the East Greenland Current: Results from the Arctic Ocean-02 Oden expedition, *J. Mar. Syst.*, *55*(1–2), 1–30, doi:10.1016/j.jmarsys.2004.06.008.

Siegert, M. J., and I. Marsiat (2001), Numerical reconstructions of LGM climate across the Eurasian Arctic, *Quat. Sci. Rev.*, *20*(15), 1595–1605, doi:10.1016/S0277-3791(01)00017-8.

Siegert, M. J., J. A. Dowdeswell, and M. Melles (1999), Late Weichselian glaciation of the Russian High Arctic, *Quat. Res.*, *52*(3), 273–285, doi:10.1006/qres.1999.2082.

Spielhagen, R. F., K. H. Baumann, H. Erlenkeuser, N. R. Nowaczyk, N. Nørgaard-Pedersen, C. Vogt, and D. Weiel (2004), Arctic Ocean deep-sea record of northern Eurasian ice sheet history, *Quat. Sci. Rev.*, *23*(11–13), 1455–1483, doi:10.1016/j.quascirev.2003.12.015.

Tachikawa, K., C. Jeandel, and M. Roy-Barman (1999), A new approach to the Nd residence time in the ocean: The role of atmospheric inputs, *Earth Planet. Sci. Lett.*, *170*(4), 433–446, doi:10.1016/S0012-821X(99)00127-2.

Tarasov, L., and W. R. Peltier (2005), Arctic freshwater forcing of the Younger Dryas cold reversal, *Nature*, *435*(7042), 662–665, doi:10.1038/nature03617.

Tarasov, L., and W. R. Peltier (2006), A calibrated deglacial drainage chronology for the North American continent: Evidence of an Arctic trigger for the Younger Dryas, *Quat. Sci. Rev.*, *25*(7–8), 659–688, doi:10.1016/j.quascirev.2005.12.006.

Teller, J. T., M. Boyd, Z. Yang, P. S. G. Kor, and A. M. Fard (2005), Alternative routing of Lake Agassiz overflow during the Younger Dryas: New dates, paleotopography, and a re-evaluation, *Quat. Sci. Rev.*, *24*(16–17), 1890–1905, doi:10.1016/j.quascirev.2005.01.008.

Tessier, A., P. G. C. Campbell, and M. Blsson (1979), Sequential extraction procedure for the speciation of particulate trace metals, *Anal. Chem.*, *51*(7), 844–851, doi:10.1021/ac50043a017.

Thirlwall, M. F. (2002), Multicollector ICP-MS analysis of Pb isotopes using a 207pb-204pb double spike demonstrates up to 400 ppm/amu systematic errors in TI-normalization, *Chem. Geol.*, *184*(3–4), 255–279, doi:10.1016/S0009-2541(01)00365-5.

Thornalley, D. J. R., I. N. McCave, and H. Elderfield (2011), Tephra in deglacial ocean sediments south of Iceland: Stratigraphy, geochemistry and oceanic reservoir ages, *J. Quaternary Sci.*, *26*(2), 190–198, doi:10.1002/jqs.1442.

von Blanckenburg, F., and T. F. Nägler (2001), Weathering versus circulation-controlled changes in radiogenic isotope tracer composition of the Labrador Sea and North Atlantic Deep Water, *Paleoceanography*, *16*(4), 424–434, doi:10.1029/2000PA000550.

White, W. M., F. Albarède, and P. Télouk (2000), High-precision analysis of Pb isotope ratios by multi-collector ICP-MS, *Chem. Geol.*, *167*(3–4), 257–270, doi:10.1016/S0009-2541(99)00182-5.

Winter, B. L., C. M. Johnson, and D. L. Clark (1997), Strontium, neodymium, and lead isotope variations of authigenic and silicate sediment components from the Late Cenozoic Arctic Ocean: Implications for sediment provenance and the source of trace metals in seawater, *Geochim. Cosmochim. Acta*, *61*(19), 4181–4200, doi:10.1016/S0016-7037(97)00215-9.

Wooden, J. L., G. K. Czamanske, V. A. Fedorenko, N. T. Arndt, C. Chauvel, R. M. Bouse, B. S. W. King, R. J. Knight, and D. F. Siems (1993), Isotopic and trace-element constraints on mantle and crustal contributions to Siberian continental flood basalts, Noril'sk area, Siberia, *Geochim. Cosmochim. Acta*, *57*(15), 3677–3704, doi:10.1016/0016-7037(93)90149-Q.

Zamelczyk, K., K. Husum, M. Hald, A. de Vernal, J. Maccali, and C. Hillaire-Marcel (2010), Changes in water mass distribution and sea ice conditions in central Fram Strait over the last 20,000 years, paper presented at 4th International Conference and Workshop Jointly With MOCA, Arct. Paleoclim. and its Extremes, Höfn, Iceland.

J. Carignan, TAKUVIK International Center for Arctic and Sub-Arctic Ecogeosystems Studies, CNRS, Centre d'études nordiques, Université Laval, local 1202, 2405 rue de la Terrasse, Québec, QC G1V 0A6, Canada. (jean.carignan@takuvik.ulaval.ca)

C. Hillaire-Marcel and J. Maccali, GEOTOP Research Center,Université du Québec à Montréal, C.P. 8888 Succ Centre Ville, Montréal, QC H3C 3P8 Canada. (chm@uqam.ca; jmaccali@crpg.cnrs-nancy.fr)

L. C. Reisberg, Centre de Recherches Pétrographiques et Géochimiques, CNRS/INSU, 15 rue Notre-Dame-des-Pauvres, B.P. 20, F-54501 Vandoeuvre lès Nancy, France. (reisberg@crpg.cnrs-nancy.fr)